The Feeding Biomechanics and Dietary Ecology of *Paranthropus boisei*

AMANDA L. SMITH,[1] STEFANO BENAZZI,[2,3] JUSTIN A. LEDOGAR,[1] KELLI TAMVADA,[1] LESLIE C. PRYOR SMITH,[4] GERHARD W. WEBER,[5] MARK A. SPENCER,[6,7] PETER W. LUCAS,[8] SHAJI MICHAEL,[9] ALI SHEKEBAN,[9] KHALED AL-FADHALAH,[10] ABDULWAHAB S. ALMUSALLAM,[11] PAUL C. DECHOW,[4] IAN R. GROSSE,[12] CALLUM F. ROSS,[13] RICHARD H. MADDEN,[13] BRIAN G. RICHMOND,[14,15,16] BARTH W. WRIGHT,[17] QIAN WANG,[18] CRAIG BYRON,[19] DENNIS E. SLICE,[5,20] SARAH WOOD,[12] CHRISTINE DZIALO,[12] MICHAEL A. BERTHAUME,[21,22] ADAM VAN CASTERN,[8,23] AND DAVID S. STRAIT[1]*

[1]Department of Anthropology, University at Albany, Albany, New York
[2]Department of Human Evolution, Max Planck Institute for Evolutionary Anthropology, Deutscher Platz 6, 04103 Leipzig, Germany
[3]Department of Cultural Heritage, University of Bologna, Via degli Ariani 1, Ravenna 48121, Italy
[4]Department of Biomedical Sciences, Texas A&M Health Science Center, Baylor College of Dentistry, Dallas, Texas
[5]Department of Anthropology, University of Vienna, Althanstr. 14, A-1090 Vienna, Austria
[6]School of Human Evolution and Social Change, Arizona State University, Tempe, Arizona
[7]Department of Biology, South Mountain Community College, Phoenix, Arizona
[8]Department of Bioclinical Sciences, Faculty of Dentistry, Kuwait University, Safat 13110, Kuwait
[9]Nanotechnology Research Facility, College of Engineering and Petroleum, Kuwait University, Safat 13060, Kuwait
[10]Department of Mechanical Engineering, College of Engineering and Petroleum, Kuwait University, Safat 13060, Kuwait
[11]Department of Chemical Engineering, College of Engineering and Petroleum, Kuwait University, Safat 13060, Kuwait
[12]Department of Mechanical & Industrial Engineering, University of Massachusetts, Amherst, Massachusetts
[13]Department of Organismal Biology & Anatomy, University of Chicago, Chicago, Illinois
[14]Center for the Advanced Study of Hominid Paleobiology, Department of Anthropology, The George Washington University, NW, Washington, District of Columbia
[15]Human Origins Program, National Museum of Natural History, Smithsonian Institution, Washington, District of Columbia
[16]Division of Anthropology, American Museum of Natural History, New York, New York
[17]Department of Anatomy, Kansas City University of Medicine and Biosciences, Kansas City, Missouri
[18]Division of Basic Medical Sciences, Mercer University School of Medicine, Macon, Georgia
[19]Department of Biology, Mercer University, Macon, Georgia
[20]School of Computational Science & Department of Biological Science, Florida State University, Dirac Science Library, Tallahassee, Florida

Additional Supporting Information may be found in the online version of this article.

Grant sponsor: National Science Foundation Physical Anthropology HOMINID program; Grant numbers: NSF BCS 0725219, 0725183, 0725147, 0725141, 0725136, 0725126, 0725122, 0725078; Grant sponsor: "Biomesh"; Grant number: NSF DBI 0743460; Grant sponsor: EU FP6 Marie Curie Actions; Grant number: MRTN-CT-2005-019564 "EVAN"; Grant sponsor: Kuwait University General Facilities Project; Grant number: GE01/07, GDO2/11.

*Correspondence to: David S. Strait, Department of Anthropology, University at Albany, 1400 Washington Avenue, Albany, NY 12222. E-mail: dstrait@albany.edu

Revised 3 October 2014; Accepted 11 October 2014.

DOI 10.1002/ar.23073

Published online 00 Month 2014 in Wiley Online Library (wileyonlinelibrary.com).

J_ID: AR Customer A_ID: AR23073 Cadmus Art: AR23073 Ed. Ref. No.: 14-0304 Date: 30-October-14 Stage: Page: 2

[21]Department of Anthropology, University of Massachusetts, Amherst, Massachusetts
[22]Medical and Biological Engineering Research Group, Department of Engineering, University of Hull, Cottingham Road, Kingston-Upon-Hull, HU6 7RX, United Kingdom
[23]Max Planck Weizman Center for Integrative Archaeology and Anthropology, Max Planck Institute for Evolutionary Anthropology, Deutscher Platz 6, 04103, Leipzig, Germany

AQ9

ABSTRACT

The African Plio-Pleistocene hominins known as australopiths evolved derived craniodental features frequently interpreted as adaptations for feeding on either hard, or compliant/tough foods. Among australopiths, *Paranthropus boisei* is the most robust form, exhibiting traits traditionally hypothesized to produce high bite forces efficiently and strengthen the face against feeding stresses. However, recent mechanical analyses imply that *P. boisei* may not have been an efficient producer of bite force and that robust morphology in primates is not necessarily strong. Here we use an engineering method, finite element analysis, to show that the facial skeleton of *P. boisei* is structurally strong, exhibits a strain pattern different from that in chimpanzees (*Pan troglodytes*) and *Australopithecus africanus*, and efficiently produces high bite force. It has been suggested that *P. boisei* consumed a diet of compliant/tough foods like grass blades and sedge pith. However, the blunt occlusal topography of this and other species suggests that australopiths are adapted to consume hard foods, perhaps including grass and sedge seeds. A consideration of evolutionary trends in morphology relating to feeding mechanics suggests that food processing behaviors in gracile australopiths evidently were disrupted by environmental change, perhaps contributing to the eventual evolution of *Homo* and *Paranthropus*. Anat Rec, 00:000–000, 2014.

Key words: geometric morphometrics; functional morphology; feeding biomechanics

Paranthropus boisei exhibits large and anteriorly placed attachments for the muscles of mastication, huge blunt premolars and molars with thick enamel, a massive mandible with a tall ramus, and visor-like zygomatics rising above the premolars (Tobias, 1967; Rak, 1983; Teaford and Ungar, 2000). Based on both comparative and mechanical grounds, these traits have traditionally been hypothesized to be adaptations for feeding on hard foods (Jolly, 1970; Lucas et al., 1985; Peters, 1987; Strait et al., 2009) but isotopic and microwear analyses have been interpreted as evidence that *P. boisei* had a diet of compliant/tough foods (Ungar et al., 2008; Van der Merwe et al., 2008; Cerling et al., 2011a; Ungar and Sponheimer, 2011). Both diets should be associated with cranial morphologies that are structurally strong and produce high bite force efficiently, but recent mechanical simulations imply that robust cranial morphology may not generate bite force efficiently (Wroe et al., 2010) nor be strong (Dumont et al., 2011b). We test the hypothesis that the cranium of *P. boisei* is configured to either reinforce the face against loads applied to the cheek teeth (Rak, 1983) or to increase the mechanical advantage of the masticatory muscles (Demes and Creel, 1988), or both. Our tests of these hypotheses entail integration (e.g., accompanying article in this issue by Smith et al., in press) of geometric morphometrics (GM) with an engineering method, finite element analysis (FEA), that is used to examine how objects of complex geometry and material properties respond to complex loads (e.g., Zienkiewicz et al., 2005). We then synthesize a range of mechanical and other data to evaluate which types of foods are most likely to have influenced the evolution of feeding adaptations in this and other hominin species.

HYPOTHESES

Rak (1983) hypothesized that the derived cranial morphology seen in *P. boisei* serves to resist loads associated with the generation of bite forces on the cheek teeth. A key variable in Rak's (1983) model is the anteroposterior placement of the zygomatic root. He hypothesizes that the anteriorly placed root in *P. boisei* plays a key role in absorbing stresses associated with loads applied to the massively enlarged premolars in this species. Moreover, the inflated zygomatic with its straight zygomaticoalveolar crest should reinforce the zygomatic arch and the entire midface against the pull of a hypertrophied masseter muscle. An implication is that the nature of the stresses and associated deformations of the face of this species may be quite different from that of

ID: chandrasekar.v Time: 20:54 I Path: N:/3b2/AR##/Vol00000/140193/APPFile/JW-AR##140193

J_ID: **AR** Customer A_ID: **AR23073** Cadmus Art: **AR23073** Ed. Ref. No.: **14-0304** Date: **30-October-14** Stage: Page: **3**

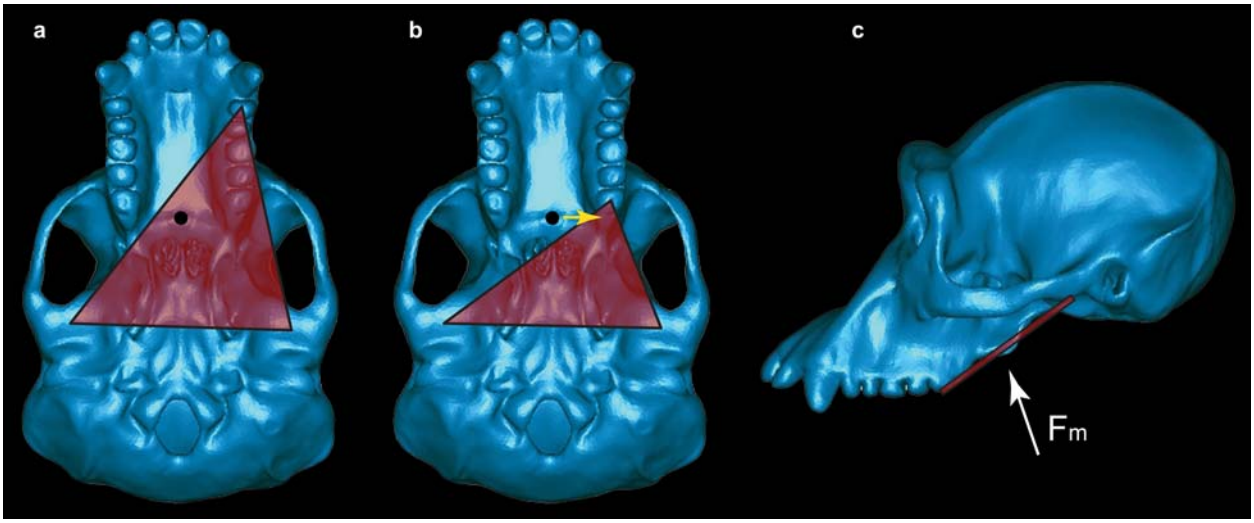

C
O
L
O
R

Fig. 1. The constrained lever model. **A**: Basal view of a chimpanzee skull illustrating the triangle of support (red) during a bite on a mesially positioned tooth. The resultant of the masticatory muscle forces is indicated by the black circle, and for simplicity is assumed in this case to be directed perpendicular to the plane of the image (but see below). The exact location of the muscle resultant cannot be known with certainty, but will be found in the midline if the muscles on the right and left sides of the body are acting with equal activity levels. Moreover, the resultant cannot be found anterior to the distal most teeth (in this case, the third molars). Thus, the resultant shown here is in its anterior-most position under the assumption that the adductor muscles are acting with bilateral symmetry. Note that the resultant in this bite falls within the triangle of support (red triangle) defined by the bite point and the two TMJs. **B**: A bite on a more distally placed tooth. The muscle resultant is now found outside the triangle. By reducing the balancing-side muscle force, it is possible to shift the position of the resultant toward the working-side (yellow arrow) so that the resultant is once again within the triangle. Note that if the resultant were to be found anterior to the bite point, it would be impossible to shift the resultant into the triangle. **C**: Lateral view of the masticatory apparatus. Note that the triangle of support (red line) is not horizontal, and that the muscle resultant (F_m, white arrow) may not be oriented perpendicular to the triangle, nor positioned in the same plane as the distal-most teeth.

other hominins and apes. Moreover, although not stated explicitly by Rak (1983), one can infer the prediction that when controlling for muscle force and bite point location, stresses in the *P. boisei* face should generally be lower than in gracile australopiths and non-human apes.

Hypotheses regarding bite force generation in *P. boisei* are complicated by the fact that there are varying levels of complexity to the biomechanical hypotheses thought to govern bite force generation in mammals. In a simple (unconstrained) lever model (e.g., Smith, 1978), *P. boisei* is predicted to have the capability of generating very high bite forces (Demes and Creel, 1988) not only because its muscles of mastication are thought to be large (and, thus, powerful), but also because the attachment sites of these muscle have been moved forward relative to the tooth row (e.g., Rak, 1983). As a result, those muscles should have a high mechanical advantage and bites on, for example, the cheek teeth should produce very high bite forces.

A complication with this scenario, however, is that there are biomechanical constraints on bite force production in mammals (including primates). The mammalian jaw functions as a Class III lever system, where the muscle force is applied between the biting tooth and the right and left temporomandibular joints (TMJs) (fulcrum): the biting tooth and the two joints define
F1 three corners of a "triangle of support" (Fig. 1). For the system to be stable, the resultant of the masticatory muscle force vectors must fall within the triangle of support. If the resultant falls outside of the triangle then one of three points will be loaded in tension as the system rotates around the other two points. When the jaw is loaded in this fashion, the working-side (i.e., biting-side) TMJ should experience a tensile reaction force that will distract the joint (i.e., separate the mandibular condyle from the articular eminence) (Greaves, 1978; Spencer, 1999). These tensile/distractive forces are hypothesized to be problematic for the TMJ because the soft tissues of this joint do not appear to be well configured to resist forces that "pull" the condyle away from the articular eminence (Greaves, 1978). Thus, during both dynamic jaw movements and static biting, this model suggests that muscles should be activated in such a way as to ensure that the muscle resultant lies within the triangle of support. This hypothesis is known as the Constrained Lever Model of jaw biomechanics (Greaves, 1978).

One effect of this constraint is that a midline muscle resultant may fall outside of the triangle as the bite point is positioned more and more distally on the tooth row (i.e., as during bites on the molar teeth). A midline resultant is obtained when the adductor muscles on both sides of the head are acting with bilateral symmetry. Thus, during bites on distal teeth (Fig. 1), it may be necessary to reduce the magnitude of the balancing-side adductor forces, thereby shifting the muscle resultant toward the working-side and maintaining the resultant within the triangle (Greaves, 1978; Spencer, 1999). The cost of this reduction is that less muscle force is available to produce bite force (e.g., Spencer, 1998; Clausen et al., 2008).

ID: **chandrasekar.v** Time: 20:54 I Path: N:/3b2/AR##/Vol00000/140193/APPFile/JW-AR##140193

J_ID: AR Customer A_ID: AR23073 Cadmus Art: AR23073 Ed. Ref. No.: 14-0304 Date: 30-October-14 Stage: Page: 4

A second complication with the need to maintain the resultant within the triangle is that bite force cannot simply be increased by shifting the adductor muscles anteriorly. As the muscles shift anteriorly, so does the muscle resultant. If the resultant were to be located anterior to the most distal teeth, then bites on them would necessarily produce distractive joint reaction forces because it would be impossible for the resultant to lie within the triangle. Thus, the muscle resultant is constrained to always be found posterior to these teeth (Greaves, 1998; Spencer, 1999).

Accordingly, the constrained lever model predicts (Greaves, 1978; Spencer, 1999) that mammals adapted to generate high bite forces on the mesial teeth (incisors, canines, premolars) should combine anteriorly placed adductor muscles with either an anteriorly shifted tooth row, or a tooth row exhibiting reduced or missing distal teeth (molars), since these configurations reduce the likelihood that the resultant will fall anterior to the most distal teeth. In contrast, mammals adapted to generate high bite forces on the distal teeth should exhibit widely separated TMJs but narrow dental arcades, since this configuration lessens the need to reduce the balancing-side muscle forces in order to shift the resultant toward the working-side. Spencer (1999) has found that the configuration of the feeding apparatus is consistent with the predictions of the constrained lever model (Greaves, 1978) across a broad sample of extant anthropoids.

P. boisei is extraordinary among primates in that it combines distally positioned molar teeth with a masseter muscle that originates far forward on the face (Rak, 1983). This configuration could make *P. boisei* especially at risk of experiencing distractive reaction forces that would put the working-side TMJ into tension during unilateral molar biting (Greaves, 1978; Spencer, 1995, 1998, 1999). Moreover, although its TMJs are widely separated (Picq, 1990), its palate is absolutely wide and certainly not relatively narrower than those of chimpanzees. Collectively, this morphology is not obviously consistent with the predictions of the Constrained Lever Model. In theory, *P. boisei* could avoid distractive forces on the TMJ by strongly reducing recruitment of the balancing-side (i.e., non-biting-side) muscles, but this would have the effect of reducing bite force magnitude. An inability to generate high bite forces on the molars would seem to be incompatible with the hypothesis that *P. boisei* was adapted to eat hard foods. Thus, we also tested whether the *P. boisei* TMJ is especially at risk of distraction.

An ability to generate high bite forces is compatible with a hard food diet, but Walker (1981) argued that high bite forces were needed not necessarily to generate high stresses within hard foods, but rather to maintain occlusal pressures across a tooth row with an expanded occlusal surface. In this scenario, australopiths had a "high volume" or "bulk feeding" diet of food tissues of varying quality and material properties. In other words, larger teeth allow more food to be processed with each chew (e.g., Lucas, 2004). A prediction of this hypothesis is that occlusal pressure is maintained as occlusal area increases in australopiths.

In summary, stress and associated strain magnitudes in the *P. boisei* face are predicted to be lower than in gracile australopiths and non-human apes, and the overall patterning of the strains should be different as well (Rak, 1983). A hard object feeding hypothesis predicts that *P. boisei* is capable of producing high bite forces efficiently, and thus should not experience limitations on the recruitment of balancing-side masticatory muscles that are greater than in other taxa. An indicator of such a limitation would be the presence of strong distractive reaction forces at the working-side TMJ. The bulk feeding hypothesis predicts that occlusal pressures in apes and early hominins should be similar despite differences in maximum bite force.

Hypotheses about feeding mechanics in *P. boisei* were tested using FEA informed by GM. A finite element model (FEM) of a well-preserved *P. boisei* cranium (OH 5) was constructed and compared to FEMs of an *Australopithecus africanus* cranium (a composite of specimens Sts 5 and Sts 52a but referred to here as Sts 5), and six chimpanzee crania representing extreme ends of the range of morphological variation in *Pan troglodytes* (Smith et al., in press). All models were loaded with bilaterally symmetrical muscle forces simulating maximal bites on the molars and premolars.

MATERIALS AND METHODS

Geometric Morphometric Analysis of Cranial Shape Variation in Pan Troglodytes

An assessment of interspecific differences in biomechanics should incorporate an understanding of the biomechanical significance of intraspecific shape variation (O'Higgins et al., 2011; Weber et al., 2011). Unfortunately, such an understanding is generally lacking with respect to primates. Although *in vivo* experimental bone strain studies typically collect data from more than one individual (e.g., Hylander et al., 1991; Hylander and Johnson, 1997; Ross et al., 2011), there is no precise understanding of how those individuals differ morphologically from each other or from other conspecifics. Moreover, practical limitations have tended to limit finite element analyses to a consideration of only a few individuals per species (Strait et al., 2005, 2009; Kupczik et al., 2007, 2009; Wroe et al., 2010; Dumont et al., 2011a, b; Weber et al., 2011; Wood et al., 2001). In order to overcome this limitation, we have used GM to identify chimpanzee crania that lie at the extremes of the ranges of morphological variation in the species (Smith et al., in press). These crania were then selected for FEA. Because the crania bracket a sizeable proportion of the morphological variation in the sample, it is possible to partially assess the biomechanical consequences of intraspecific shape variation without having to build FEMs of an impractically large number of specimens.

Our GM methods have been described in full elsewhere (Smith et al., in press). Briefly, as part of a previous study (Benazzi et al., 2011), 709 cranial landmarks and semilandmarks were digitized from three-dimensional surfaces derived from the computed tomography (CT) scans of 21 adult chimpanzees sampled from at least two subspecies. The (semi)landmark configurations were converted to shape coordinates by Generalized Procrustes Analysis (GPA) and using Principal Components Analysis (PCA), shape variability was decomposed into orthogonal axes. The specimens with the strongest positive and negative loadings along the first three PCs and whose CT scans were suitable for finite element modeling were selected for FEA, and

ID: chandrasekar.v Time: 20:54 I Path: N:/3b2/AR##/Vol00000/140193/APPFile/JW-AR##140193

J_ID: AR Customer A_ID: AR23073 Cadmus Art: AR23073 Ed. Ref. No.: 14-0304 Date: 30-October-14 Stage: Page: 5

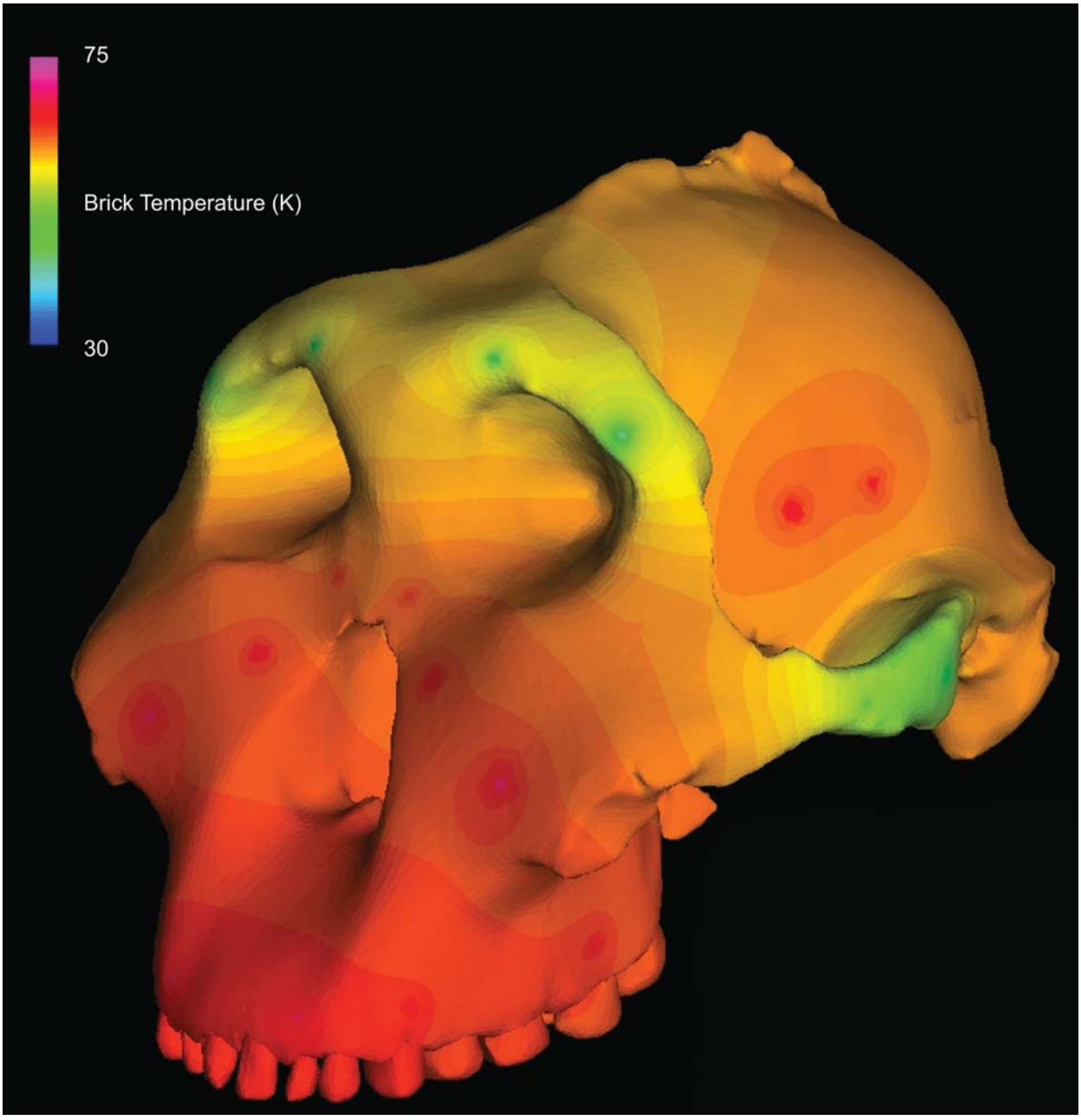

COLOR

Fig. 2. Thermal diffusion of elastic modulus through the cranium of OH 5. "Warm" colors depict regions of high stiffness, while "cool" colors depict regions of lower stiffness.

those specimens are designated PC1+, PC1−, PC2+, PC2−, PC3+, and PC3−, respectively. However, it is important to note that the specimens do not fall exactly on any given axis, and they represent real crania rather than those that have been warped along the trajectory of an axis (O'Higgins et al., 2011). Moreover, we cannot be certain that the first three principal components are the ones that are most functionally significant. Rather, our selection process merely ensures that the specimens selected for FEA represent a large range of shape diversity found in real crania; they are not being selected because of any *a priori* functional considerations.

Finite Element Model Creation

Again, methods for the creation of FEMs of chimpanzee crania identified through GM have been described in full elsewhere (Smith et al., in press). To summarize, a combination of automatic thresholding algorithms and manual slice-by-slice segmentation was used to capture the geometry of each specimen from CT data using medical imaging software. This created surface meshes comprised of thousands of tetrahedral elements that were exported as binary STL (stereolithography) files and edited in surface editing software. During this stage,

ID: chandrasekar.v Time: 20:54 I Path: N:/3b2/AR##/Vol00000/140193/APPFile/JW-AR##140193

J_ID: AR Customer A_ID: AR23073 Cadmus Art: AR23073 Ed. Ref. No.: 14-0304 Date: 30-October-14 Stage: Page: 6

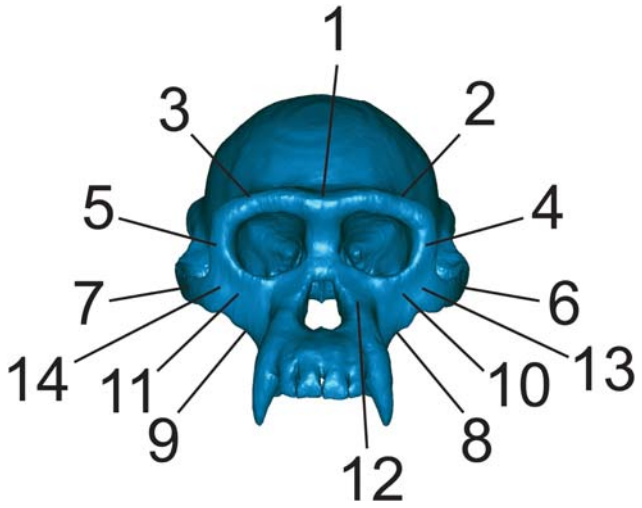

COLOR

Fig. 3. Key to regions where strains were sampled in FEMs. 1 = Dorsal interorbital. 2 = Working-side dorsal orbital. 3 = Balancing-side dorsal orbital. 4 = Working-side postorbital bar. 5 = Balancing-side postorbital bar. 6 = Working-side zygomatic arch. 7 = Balancing-side zygomatic arch. 8 = Working-side zygomatic root. 9 = Balancing-side zygomatic root. 10 = Working-side infraorbital. 11 = Balancing-side infraorbital. 12 = Working-side nasal margin. 13 = Working-side zygomatic body. 14 = Balancing-side zygomatic body.

surface models were made to be watertight volumetric solids and the geometry was refined to ensure that embedded layers of material (such as trabecular bone and pneumatized spaces) were not exposed, protruding, or distorted. Upon successful surface meshing, the models were volume meshed while maintaining triangle edge length from previous steps and controlling aspect ratio. Volume meshes were then imported into FEA software for boundary condition application and analysis.

Model creation of OH 5 and a composite of Sts 5 and Sts 52a were similar, except that the specimens were virtually reconstructed prior to mesh construction. These virtual reconstructions have previously been described (Strait et al., 2009; Benazzi et al., 2011), although the composite *A. africanus* reconstruction has been improved slightly. Namely, the positioning of the teeth has been altered following new considerations of the spatial positioning of the dentition in Sts 52a and b, whose dental arches have been functionally restored based on information preserved in the occlusal macrowear pattern (Benazzi et al., 2013). Sinuses and cavities were imported as separate surface files and merged with the model of the cranial bone. Surface files of trabecular bone in OH 5 were also merged with that model, but surfaces representing trabecular volumes were approximated in Sts 5 due to the difficulty in visualizing trabecular volumes in that specimen. The teeth and roots of Sts 52a and OH 5 were also segmented and used to generate separate volumes representing periodontal ligaments, but our prior research (Wood et al., 2011) has shown that the modeling of these tissues has a minor to negligible effect on cranial strain patterns away from the alveolus, so these structures were not modeled in this study (i.e., the tooth roots are fused with the alveolus).

Bone Material Properties

The material properties of cortical cranial bone were modeled as the average values collected from one chimpanzee cranium and one gorilla cranium (both fresh frozen) using ultrasonic techniques (Schwartz-Dabney and Dechow, 2002, 2003), as in the work by Smith et al. (in press: Table 2). Using the averaged African apes values as a guide, spatially heterogeneous isotropic material properties were assigned to the models using a thermal diffusion method in which elastic moduli are smoothly diffused through a skull as heat diffuses through an object (Davis et al., 2011) (Fig. 2). T2 F2

Muscle Forces

Muscle forces representing the anterior temporalis, superficial and deep masseters, and the medial pterygoid were applied to each FEM. These are the muscles that are most active at the instant of centric occlusion (approximated as the instant of peak strain in the mandibular corpus [e.g., Strait et al., 2005, 2007, 2008, 2009, 2010]). Force magnitude was estimated using muscle physiological cross-sectional area data (PCSA), which were obtained from dissection of a female chimpanzee (Strait et al., 2009). The PCSA data used here are consistent with those obtained by Taylor and Vinyard (2013) in a larger sample of specimens. In the past we have attempted to simulate muscle activity levels characteristic of chewing using electromyography (EMG) data gathered from *in vivo* feeding experiments (Strait et al., 2005, 2007, 2008, 2009; Nakashige et al., 2011). However, we do not currently have EMG data from chimpanzees (although these will be gathered in the future). Thus, the muscles are modeled here as being bilaterally symmetric and at a 100% activity level. Such loads would approximate a maximal, static bite.

Muscle forces were applied in all chimpanzee and hominin models by scaling the PCSA values by bone volume in each cranium to the 2/3 power. This ensures that larger models experience larger muscle forces; however the purpose of this approach is not to estimate true muscle forces in each of our models. Rather, this scaling procedure allows us to eliminate cranial size as a variable affecting strains. Thus, the differences in strain in our models only reflect differences in shape, and do not reflect differences in size (Dumont et al., 2009). This allows for an assessment of structural strength. The muscle force vectors were oriented to run from origin to insertion while wrapping around curved bone surfaces (Grosse et al., 2007). It is important to point out that because OH 5 does not have an associated mandible, we used a slightly scaled surface scan of the Peninj fossil mandible to guide our focal coordinates of muscle insertions.

Constraints

Boundary conditions were defined to constrain movement at the articular eminences of the TMJs and a bite point. In all simulations, the working-side TMJ was constrained in all directions and the balancing-side TMJ was constrained in the vertical and antero-posterior directions. In half of the simulations, the center of the

ID: chandrasekar.v Time: 20:55 I Path: N:/3b2/AR##/Vol00000/140193/APPFile/JW-AR##140193

J_ID: AR Customer A_ID: AR23073 Cadmus Art: AR23073 Ed. Ref. No.: 14-0304 Date: 30-October-14 Stage: Page: 7

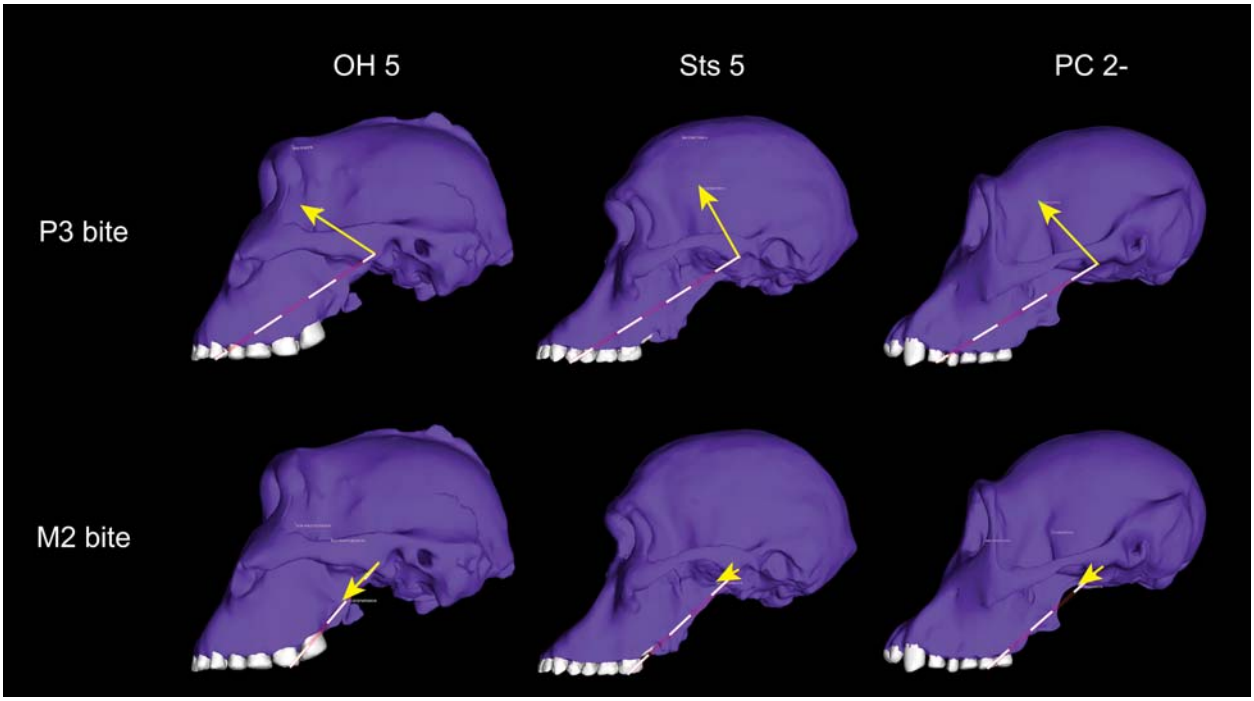

COLOR

Fig. 4. Orientation of the joint reaction force at the working-side TMJ. Forces are shown in *P. boisei* (OH 5), *A. africanus* (Sts 5), and one of the *P. troglodytes* models whose reaction forces were similar to those in the hominins (PC 2−). Yellow arrows indicate direction of the joint force. The length of the arrows is proportional to their magnitude. Dashed lines indicate the plane of the triangle of support. During premolar bites, the joint force is oriented superiorly and anteriorly into the articular eminence, reflecting the fact that the resultant of all of the muscle forces falls within the triangle. During molar biting, the reaction force in all three models is roughly parallel to the triangle, indicating that the resultant is found at approximately the edge of the triangle. Reductions in balancing-side muscle force should move the resultant into the triangle, and re-direct the joint force into the eminence. Joint force orientation in the hominins is similar to chimpanzees despite the fact that the zygomatic root has migrated forward in the former, as is evident in these specimens.

upper second molar was constrained in the vertical direction, while in a second round of simulations the center of the third premolar was similarly constrained. These minimal constraints (Dumont et al., 2005; see also Strait et al., 2005) prevent the model from experiencing rigid body motion and simulate occlusal and mandibular contacts such that when applied muscle forces pull inferiorly on the model, reaction forces are generated at each constraint. The reaction force at the bite point represents the bite force.

Data Collection

Here we report strains rather than stresses because these are easier to contextualize within the broader primate experimental strain database (e.g., Hylander et al., 1991; Ross et al., 2011). All of these strains occur at each material point of the models simultaneously. There are two types of strain: normal strains stretch or compress the material in a given direction, while shear strains distort the material in a given plane. Maximum principal strain is the maximum value of normal strain at a given material point and is tensile (i.e., positive), unless the material is in a state of tri-axial compression. Minimum principal strain is the minimum value of normal strain at the same material point and is compressive (i.e., negative), unless the material is in a state of tri-axial tension. Maximum and minimum principal strains are oriented along principal axes that are orthogonal to each other. Strain mode is the absolute value of the ratio of maximum to minimum principal strain, which describes the degree to which a given material point is primarily in tension, compression, or shear (when the principal compressive and tensile strains are equal or nearly so). Maximum shear strain is, as the name implies, the maximum value of shear experienced at a given material point, and is calculated as maximum minus minimum principal strain. Von Mises strain is a measure of distortional strain, meaning non-isometric deformation (i.e., a solid rubber ball thrown into the ocean experiences ever greater compression on all sides as it sinks but remains perfectly spherical, and thus does not experience any von Mises strain). Von Mises strain corresponds to von Mises stress, which is the metric governing the yielding of ductile materials such as bone (Keyak and Rossi, 2000). Thus, it is the strain metric that is arguably most relevant to bone strength. Strain energy density (SED) is the area underneath the stress–strain curve at any given material point and represents the strain energy per unit volume at a material point. Strain energy (SE) is the integral (i.e., volumetric sum) of SED over the volume of the model. Thus, SED provides information about where SE is being stored in an object. Maximum principal strain, minimum principal strain, strain mode, maximum shear strain, and von Mises strain can be directly calculated from strain

ID: chandrasekar.v Time: 20:55 I Path: N:/3b2/AR##/Vol00000/140193/APPFile/JW-AR##140193

J_ID: AR Customer A_ID: AR23073 Cadmus Art: AR23073 Ed. Ref. No.: 14-0304 Date: 30-October-14 Stage: Page: 8

TABLE 1. Component of the reaction force at the working-side TMJ perpendicular to the triangle of support (the plane defined by the two TMJs and the bite point)[a]

Species	Specimen	Force (P^3 bite) (N)	Force (M^2 bite) (N)
P. boisei	OH 5	885.4	57.9
A. africanus	Sts 5	455.3	43.1
P. troglodytes	PC 1−	429.2	104.9
P. troglodytes	PC 1+	466.9	136.6
P. troglodytes	PC 2−	308.8	35.6
P. troglodytes	PC 2+	345.8	77.1
P. troglodytes	PC 3−	373.9	−12.7
P. troglodytes	PC 3+	398.7	26.0

[a]Positive values are compressive and negative values are distractive.

measurements (using strain gages or full-field strain measurement techniques) and thus form the basis of *in vivo* and *ex vivo* bone strain studies.

Overall strain patterns are depicted in color maps in which gradations in color correspond to gradations in strain magnitude. These color maps summarize huge amounts of quantitative data (strain values at thousands of elements) but in practice are qualitative tools for assessing strain patterns. Quantitative strain data were collected at a small number of elements, each representing either a location at which strain data have been collected from gages in *in vivo* feeding experiments (e.g., Hylander et al., 1991), or in a region relevant to evaluating strain patterns in early hominins and extant apes (Fig. 3). F3

Bite force magnitude was recorded at the bite point constraints during both premolar and molar biting. Because the models are constrained at single nodes, bite force magnitude is simply the magnitude of the reaction force vector at those nodes. In order to determine whether the reaction force at the working-side TMJ was distractive or compressive in each model, a reference plane was defined in which two of the three axes were parallel to the triangle of support. The component of the reaction force vector orthogonal to that plane was then recorded. If the magnitude of that component was positive, then the reaction force was compressive. Inversely, if the component was negative, then the reaction force was distractive (see Clausen et al. (2008) for an analogous approach).

RESULTS

TMJ Reaction Force

During premolar bites, all models exhibited strongly compressive reaction forces at the working-side TMJ (Fig. 4, Table 1), indicating that the muscle resultant T1 F4 falls well within the triangle of support, as predicted by the constrained lever model (Fig. 1).

OH 5 was no more at risk of putting its working-side TMJ into tension during molar biting than chimpanzees and Sts 5: its working-side TMJ experiences a weakly compressive joint reaction force during unilateral molar biting with bilaterally symmetrical muscle forces (Table 1). However, during molar bites, the joint reaction force at the working-side TMJ in *P. boisei* is essentially parallel to the triangle of support, indicating that the resultant is just on the edge of the triangle. The orientation of the joint reaction force observed in OH 5 is similar to that in Sts 5 and some chimpanzees (Fig. 4). Chimpanzee reaction forces are variable, with some individuals having somewhat compressive reaction forces and other individuals having very weakly distractive forces (Table 1). It is unsurprising that bilaterally symmetric muscle forces produce distractive joint forces during molar bites in some individuals. A joint force that is directed anteriorly and inferiorly like that seen in the OH 5 model might be a threat to joint integrity, and in this regard, it was observed that when the balancing-side muscle forces were decreased in our *P. boisei* FEA, the compressive component of the working-side TMJ reaction force increased, thereby orienting the reaction force more directly into the articular eminence. Indeed, in life, we expect that in regular, dynamic mastication, or static bites the muscles of mastication in all individuals may be activated with a working-to-balancing-side asymmetry, as is often observed in other primates (Hylander et al., 1998, 2004). Notably, during maximal static bites humans exhibit an asymmetry that probably serves to maintain a safety factor protecting the working-side TMJ from distraction (Spencer, 1998). It is reasonable to hypothesize that chimpanzees, *A. africanus* and *P. boisei*, would be similar to humans in this regard, although it is not possible to estimate precisely how much of an asymmetry would be needed to ensure a sufficient safety factor in each species.

Strain

As a generalization, the chimpanzee FEMs exhibit considerable variation in strain magnitude (Fig. 5) but F5 exhibit broad similarities in the distribution of strain concentrations (Figs. 6 and 7) (Smith et al., in press). F6 F7 In some regions, the strain modes are consistently compressive or tensile, but in other regions the modes are variable between individuals (Tables 2 and 3). T3 These chimpanzees were intentionally selected to represent individuals that differed greatly in cranial shape (Smith et al., in press), so these results document the biomechanical consequences of intraspecific shape variation. Based on these findings, one might predict that even large-scale differences in cranial shape within hominin species could produce broad commonalities with respect to at least the spatial patterning of strains. However, chimpanzees exhibit notable variation in strains in the zygomatic arch and the adjacent zygomatic root. In most specimens, strains in the arch (Regions 6 and 7 in Fig. 3) are high, but in two specimens strains in the arch are lower than in the adjacent zygomatic root (Regions 8 and 9 in Fig. 3), which exhibits the highest strains of all the regions sampled in those individuals.

Strains in the *A. africanus* composite FEM broadly resemble those of chimpanzees in mode, magnitude, and distribution (Figs. 6 and 7), with two notable exceptions. First, strain magnitudes in the body of the zygomatic on the working-side (Region 13 in Fig. 3; see also Figs. 6 and 7) at the junction of the zygomatic arch and frontal process are low whereas they are comparatively higher in chimpanzees. Evidently, this portion of the midface is

ID: chandrasekar.v Time: 20:55 I Path: N:/3b2/AR##/Vol00000/140193/APPFile/JW-AR##140193

J_ID: AR Customer A_ID: AR23073 Cadmus Art: AR23073 Ed. Ref. No.: 14-0304 Date: 30-October-14 Stage: Page: 9

TABLE 2. Strain[a] and strain energy density results from simulated premolar bites

Location[b]	Specimen	Max Prin (με)	Min Prin (με)	Mode	Max shear (με)	von Mises (με)	SED (J/mm^3)
1. Dorsal interorbital	OH5	182	−72	2.53	254	238	0.24
	Sts5	186	−93	2.00	279	243	0.29
	Chimp range	118–216	−48 to −125	1.31–3.17	171–288	160–271	0.10–0.34
2. Working dorsal orbital	OH5	59	−29	2.03	88	78	0.02
	Sts5	119	−99	1.20	218	189	0. 13
	Chimp range	16–138	−21 to −88	0.61–2.27	37–199	32–189	0.00–0.14
3. Balancing dorsal orbital	OH5	118	−42	2.81	160	154	0. 10
	Sts5	102	−38	2.68	140	136	0. 07
	Chimp range	106–197	−48 to −101	1.89–3.10	153–291	146–268	0.08–0. 28
4. Working postorbital bar	OH5	189	−99	1.90	288	264	0. 26
	Sts5	581	−412	1.41	993	872	2. 76
	Chimp range	150–455	−168 to −481	0.89–1.42	318–935	276–810	0.27–2.33
5. Balancing postorbital bar	OH5	388	−163	2.38	551	513	1.08
	Sts5	910	−402	2.26	1,312	1,217	5.92
	Chimp range	370–769	−184 to −479	1.41–2.43	553–1,248	504–1,115	0.99–4.56
6. Working mid-zygo arch	OH5	232	−312	0.74	544	480	0.82
	Sts5	856	−1,135	0.75	1,991	1,784	11.26
	Chimp range	337–1710	−492 to −3,390	0.36–1.63	859–5,006	757–4,791	2.04–83.65
7. Balancing mid-zygo arch	OH5	292	−350	0.83	642	566	1.13
	Sts5	1,044	−2,255	0.46	3,299	3,164	36.73
	Chimp range	417–1,994	−179 to −2,683	0.39–2.99	713–3,958	686–3,549	1.71–53.64
8. Working zygo root	OH5	249	−522	0.48	771	694	2.00
	Sts5	449	−1,000	0.45	1,449	1,300	7.50
	Chimp range	245–537	−514 to −979	0.34–0.76	905–1,339	788–1,202	2.26–7.50
9. Balancing zygo root	OH5	179	−130	1.38	309	272	0.27
	Sts5	120	−441	0.27	561	520	1.52
	Chimp range	101–347	−275 to −539	0.35–1.15	387–693	350–644	0.64–3.03
10. Working infraorbital	OH5	388	−295	1.32	683	595	1.27
	Sts5	472	−216	2.19	688	636	1.60
	Chimp range	385–575	−211 to −479	1.06–1.82	762–1,054	560–916	1.12–2.99
11. Balancing infraorbital	OH5	341	−252	1.35	593	520	0.97
	Sts5	480	−182	2.64	662	635	1.62
	Chimp range	199–477	−146 to −351	1.21–2.05	346–828	304–722	0.33–1.92
12. Working nasal margin	OH5	176	−455	0.39	631	607	1.46
	Sts5	407	−1,213	0.34	1,620	1,600	10.29
	Chimp range	207–356	−463 to −891	0.35–0.66	679–1242	625–1183	1.54–5.60
13. Working zygo body	OH5	323	−128	2.52	451	425	0.75
	Sts5	454	−229	1.98	683	632	1.50
	Chimp range	536–994	−375 to −593	1.27–1.83	911–1576	793–1,424	2.38–7.45
14. Balancing zygo body	OH5	294	−112	2.63	406	386	0.61
	Sts5	585	−293	2.00	878	783	2.57
	Chimp range	343–1,506	−198 to −739	1.27–3.15	520–2,245	502–2,048	0.90–16.48

[a]Max Prin = maximum principal strain, Min Prin = minimum principal strain, Mode = the absolute value of Max Prin/Min Prin, Max Shear = maximum shear strain, Von Mises = von Mises strain, SED = strain energy density, Chimpanzee data from Smith et al. (2014).
[b]Locations numbered as in Fig. 3.

more rigid in Sts 5 than in *P. troglodytes*. Second, strains are higher along the nasal margin in Sts 5 than in any of the chimpanzees or OH 5.

Strains at homologous locations in the FEMs are generally lower in *P. boisei* than in *A. africanus* and *P. troglodytes* (Fig. 5; Tables 2 and 3), even with muscle and T4 bite forces twice as high or greater in *P. boisei* (Table 4). Although some chimpanzees exhibit lower strains than OH 5 at selected locations, none of the chimpanzees or Sts 5 exhibit the consistently low strains seen in the robust australopith. Thus, the face of *P. boisei* is extremely rigid in proportion to the loads that it absorbs. Moreover, the distribution of strain concentrations in the mid-face of *P. boisei* is obviously different from that seen in *P. troglodytes* and *A. africanus* (Figs. 6 and 7). In the latter two species, there is a patch of low strain directly below the orbits that is surrounded by regions of high strain. In contrast, in OH 5, there is a patch of high strain below the orbits that is bounded on several sides by areas of lower strain. This contrast is particularly evident during premolar biting. Thus, whereas the face of *A. africanus* deforms in approximately the same manner as *P. troglodytes*, the face of *P. boisei* deforms in a notably different manner. More specifically, the rostrum in *P. boisei* shears in frontal planes against a laterally placed zygomatic root rather than in parasagittal planes against a posteriorly placed midface as in *A. africanus* and *P. troglodytes*.

Bite Force, Occlusal Pressure, and Mechanical Advantage

Bite forces are higher in OH 5 than in the other models (Fig. 8; Table 4). Indeed, maximum bite force at the F8

ID: chandrasekar.v Time: 20:55 I Path: N:/3b2/AR##/Vol00000/140193/APPFile/JW-AR##140193

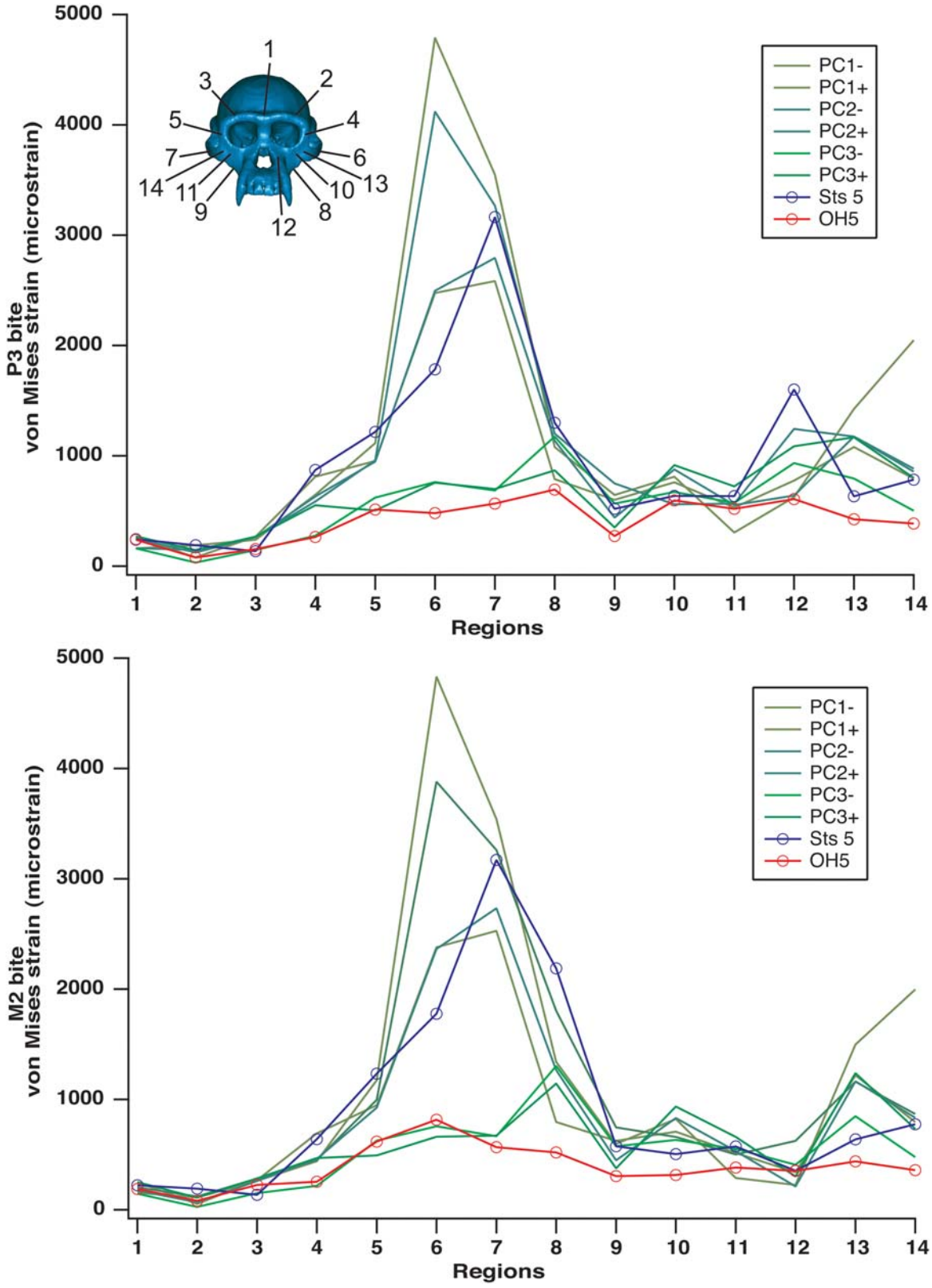

C
O
L
O
R

Fig. 5. Hominin cranial strain in comparative context. Von Mises strain recorded during premolar (P^3) and molar (M^2) biting at homologous landmarks on FEMs of six chimpanzee crania, a composite cranium of *A. africanus* labeled Sts 5, and OH 5 (*P. boisei*). The chimpanzee crania, representing actual specimens rather than morphed surface models, have been given labels corresponding to their position along the first three principal components in shape space (Supporting Information Figs. A1 and A2). PC1− and PC1+ refer to the crania at opposite extremes of the first principal component, PC2− and PC2+ are at the extremes of the second principal component, and PC3− and PC3+ are at the extremes of the third. Locations of numbered landmarks indicated on cranium. AQ8

J_ID: AR Customer A_ID: AR23073 Cadmus Art: AR23073 Ed. Ref. No.: 14-0304 Date: 30-October-14 Stage: Page: 11

P^3 in OH 5 is greater than that at the M^2 in any of the chimpanzees and Sts 5, which is remarkable given the differences in the load arms of these two bite points. Bite forces in Sts 5 (a presumed small female) are within the chimpanzee range, but larger than those produced by all but the largest chimp males (PC3+, PC3−). Our bite force estimates in Sts 5 are higher than in our previous study of this specimen (Strait et al., 2009), but that earlier study underestimated muscle force magnitude and assumed muscle force orientations without the benefit of an articulated mandible. Moreover, the current bite force estimates correspond extremely well with estimates generated by Eng et al. (2013) using different methods. Our estimates of bite force at M^2 in OH 5 and Sts 5 are only 5% and 6% larger than theirs, respectively, and their average value for chimpanzees falls within our range. In contrast, a prior simulation by another research group (Wroe et al., 2010) found that OH 5 produced bite forces somewhat greater than those in simulations of extant hominoids (including the much larger *Gorilla*), but that the maximum molar bite force estimate was roughly half that observed here (see below). That study also found that Sts 5 produced bite forces that were lower than those of all other great apes. Thus, our bite force estimates are higher but we are not aware of any independent experimental bite force data that are incompatible with our results. Our prior (Strait et al., 2009) estimates of normal and maximum bite force in macaques were within 10% of values obtained from *in vivo* experiments (Hylander, 1979), and both our current estimates of maximum bite force in OH 5 and Sts 5 and those of Eng et al. (2013) correspond roughly with independently obtained values estimated from tooth mechanics for *P. boisei* and *A. africanus*, respectively (Constantino et al., 2010).

P. boisei was able to generate high bite forces at both the mesial (P^3) and distal (M^2) ends of the postcanine tooth row but produced pressures across tooth occlusal surfaces that were only at the bottom of the range observed in chimpanzees (Table 4); pressure at the second molar in OH 5 is roughly equivalent to that of a small female chimpanzee (PC1+) and only 72% of that of the chimpanzee mean. Pressures in *A. africanus* were even lower. Results obtained here on occlusal pressure are very similar to those obtained by Eng et al. (2013)

The efficiency of biting can be assessed by considering mechanical advantage (MA) (Table 4). During bites on the third premolar, the MA of OH 5 is comparable to that of *P. troglodytes*, despite the fact that its premolar load arm is longer. Thus, *P. boisei* increased the lever arm of its muscle resultant (the vector sum of all muscle forces), thereby maintaining efficiency along the mesially expanded portion of its tooth row. During a bite on the second molar, MA in OH 5 is well above the chimpanzee range and exceeds that of *A. africanus*. Thus, *P. boisei* was an efficient producer of molar bite force. Without such efficiency (e.g., Wroe et al., 2010), occlusal pressures across the expanded tooth surface would have been very low.

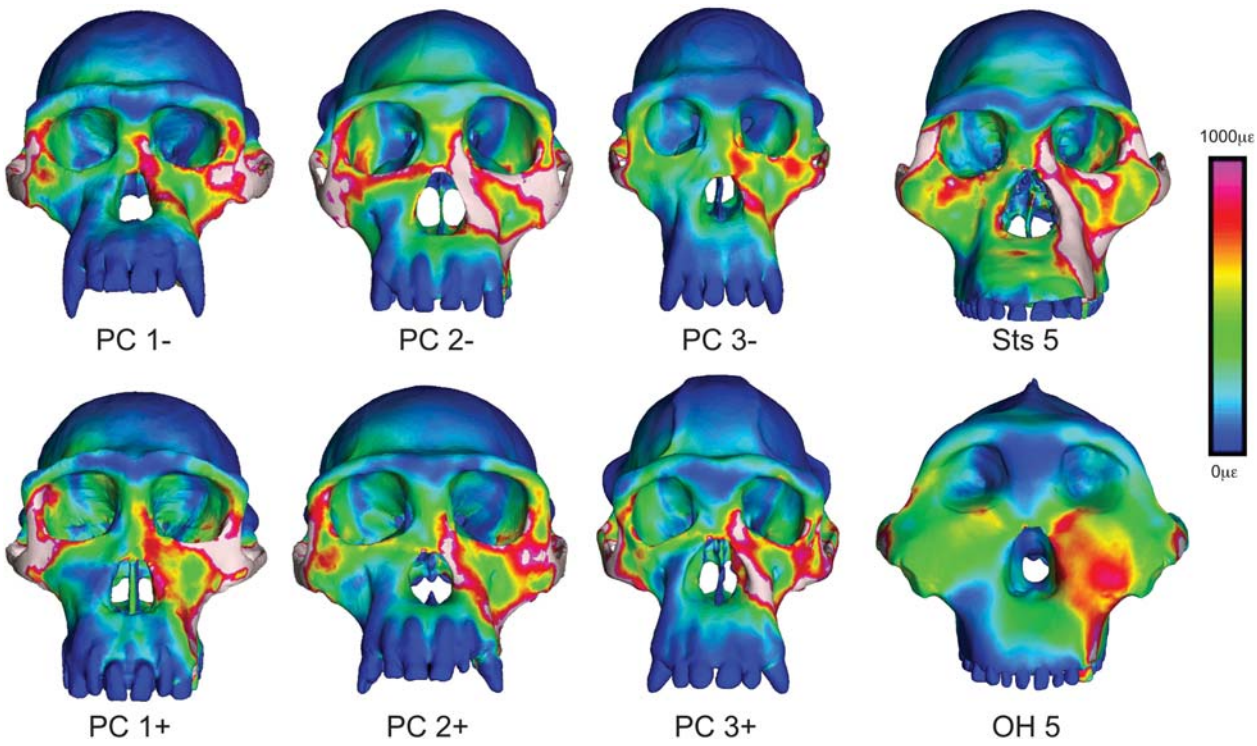

C O L O R

Fig. 6. Visualization of strain during premolar biting. Color mapping of von Mises strain in FEMs of the crania of *P. troglodytes, A. africanus*, and *P. boisei* during simulated bites on the left third premolar. Crania are scaled to the same height to visually accentuate differences in shape. White regions indicate areas where strains exceed 1,000 microstrain.

ID: chandrasekar.v Time: 20:56 I Path: N:/3b2/AR##/Vol00000/140193/APPFile/JW-AR##140193

J_ID: AR Customer A_ID: AR23073 Cadmus Art: AR23073 Ed. Ref. No.: 14-0304 Date: 30-October-14 Stage: Page: 12

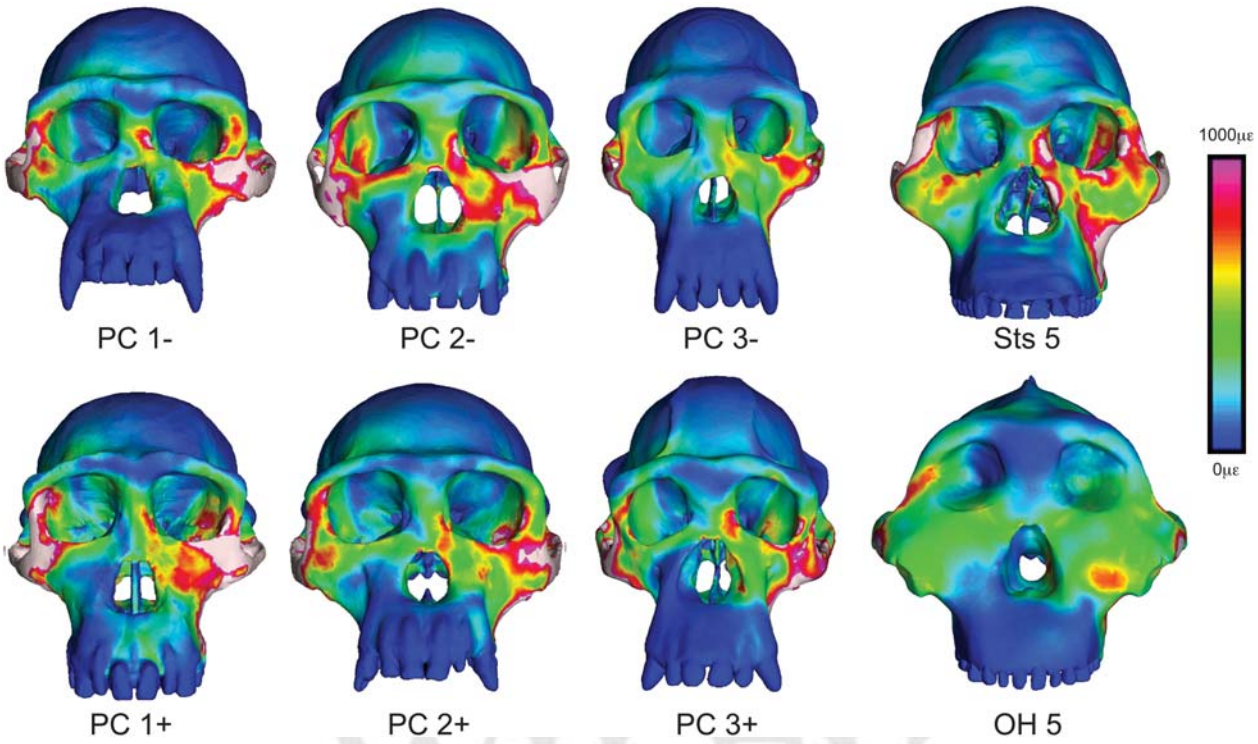

COLOR

Fig. 7. Visualization of strain during molar biting. Color mapping of von Mises strain in FEMs of the crania of *P. troglodytes, A. africanus*, and *P. boisei* during simulated bites on the left second molar. Crania are scaled to the same height to visually accentuate differences in shape. White regions indicate areas where strains exceed 1,000 microstrain.

DISCUSSION

Geometric Morphometrics in Functional Morphology

The role of GM in the present study is critical. By identifying and modeling chimpanzee specimens at the extreme ends of variation, it is possible to assess the mechanical consequences of intraspecific variation (Smith et al., in press). These data provide the context for interpreting interspecific mechanical differences among and between australopiths and apes. Smith et al. (in press) found that chimpanzee crania differing substantially in shape exhibit strong variation in strain magnitudes at several locations across the face, but that the spatial distribution of strain concentrations was conservative. In this context, it is clear that the strains in OH 5 differ from those in Sts 5 and *P. troglodytes*. Strain magnitudes at select locations (Tables 2 and 3) in OH 5 fall at or below those seen in the other models, and these values represent only a small fraction of the strain data contained within the FEMs. Qualitatively, it appears that strains are notably lower in OH 5 across large areas of the face (Figs. 6 and 7). Moreover, the patterning of strains in OH 5 is clearly different (Figs. 6 and 7) in relation to the variation seen within chimpanzees. It is the chimpanzee data that allow the conclusion that OH 5 is mechanically distinct.

In addition, the chimpanzee data allow the identification of fine-scale differences between Sts 5 and *P. troglodytes*. Overall, there are many qualitative and quantitative similarities among the crania examined here (Figs. 5–7). One notable difference is that the zygomatic body is structurally stiffer in Sts 5 than in chimpanzees on the working-side during biting. At present, it is difficult to discern whether or not this difference is adaptively significant. One possible explanation might be that feeding behaviors in *A. africanus* routinely require bites that are either high in magnitude or highly repetitive, and that the zygomatic body adapted by becoming stronger. However, other aspects of the craniofacial skeleton evidently do not require such an adaptive response (for e.g., Sts 5 experiences very high strains in the zygomatic arch), so this explanation seems incomplete. Another explanation could be that the morphology of the zygomatic in *A. africanus* is related to increasing the leverage of the masseter muscle, and that the lower strains seen in Sts 5 are a non-adaptive consequence of this morphology. Alternatively, the morphology of the zygomatic may be adapted not to reduce stress and strain in the zygomatic bone, but rather in the adjacent zygomatico-maxillary suture. Although the suture is not modeled here, in most chimpanzee specimens its path seems likely to run through or next to regions of the facial skeleton that experience high strains. This seems less likely to be the case in Sts 5 for at least the inferolateral portion of the suture. Patent sutures fail at relatively modest stress levels (e.g., Popowics and Herring, 2007), so it is possible that some stress-reducing cranial structures serve to shield sutures rather than bone (Wang et al., 2012).

Sts 5 also differs from chimpanzees in that it exhibits higher strains along the working-side nasal margin

ID: chandrasekar.v Time: 20:56 I Path: N:/3b2/AR##/Vol00000/140193/APPFile/JW-AR##140193

TABLE 3. Strain[a] and strain energy density results from simulated molar bites

Location[b]	Specimen	Max Prin (με)	Min Prin (με)	Mode	Max shear (με)	von Mises (με)	SED (J/mm^3)
1. Dorsal interorbital	OH5	145	−55	2.64	200	187	0.15
	Sts5	172	−81	2.12	253	222	0.24
	Chimp range	108–198	−45 to −76	1. 46–3.10	153–270	145–250	0.08–0.28
2. Working dorsal orbital	OH5	61	−29	2.10	90	81	0.03
	Sts5	118	−102	1.16	220	191	0.13
	Chimp range	5–81	−22 to −91	0.23–2.18	27–138	26–120	0.00–0.07
3. Balancing dorsal orbital	OH5	171	−57	3.00	228	225	0.20
	Sts5	102	−39	2.62	141	136	0.07
	Chimp range	110–209	−46 to −111	1.80–3.08	156–310	150–284	0.09–0.31
4. Working postorbital bar	OH5	177	−103	1.72	280	254	0.24
	Sts5	357	−381	0.94	738	640	1.45
	Chimp range	93–365	−150 to −431	0.62–1.21	243–796	216–692	0.17–1.70
5. Balancing postorbital bar	OH5	476	−176	2.70	652	617	1.61
	Sts5	935	−381	2.45	1316	1234	6.20
	Chimp range	413–817	−169 to −492	1.43–2.54	536–1309	492–1175	0.97–5.08
6. Working mid-zygo arch	OH5	379	−534	0.71	913	815	2.36
	Sts5	875	−1,115	0.78	1,990	1,776	11.19
	Chimp range	293–1,629	−445 to −3,416	0.37–1.62	737–5,039	662–4,832	1.57–84.99
7. Balancing mid-zygo arch	OH5	283	−357	0.79	640	567	1.14
	Sts5	1,064	−2,253	0.47	3,317	3,171	36.81
	Chimp range	405–1,955	−172 to −2,675	0.39–3.00	686–3,950	666–3,542	1.61–53.31
8. Working zygo root	OH5	278	−321	0.87	599	520	0.96
	Sts5	718	−1721	0.42	2,439	2,188	22.51
	Chimp range	350–570	−523 to −1,061	0.38–0.74	910–1,475	795–1,803	2.30–8.41
9. Balancing zygo root	OH5	219	−121	1.81	340	305	0.36
	Sts5	127	−494	0.26	621	576	1.93
	Chimp range	108–351	−288 to −607	0.28–1.14	415–843	375–747	0.72–1.95
10. Working infraorbital	OH5	242	−91	2.66	333	314	0.42
	Sts5	360	−195	1.85	555	504	0.96
	Chimp range	438–578	−227 to −498	1.16–2.06	718–1,076	632–935	1.51–3.11
11. Balancing infraorbital	OH5	257	−174	1.48	431	383	0.53
	Sts5	445	−141	3.16	586	574	1.39
	Chimp range	191–448	−135 to −307	1.21–2.21	325–754	287–660	0.30–1.63
12. Working nasal margin	OH5	136	−245	0.56	381	352	0.45
	Sts5	134	−248	0.54	382	354	0.46
	Chimp range	111–254	−119 to −457	0.49–1.19	244–681	211–625	0.17–1.51
13. Working zygo body	OH5	331	−172	1.92	503	438	0.90
	Sts5	460	−231	1.99	691	638	1.54
	Chimp range	566–993	−408 to −572	1.34–1.77	974–1,697	847–1497	2.71–8.07
14. Balancing zygo body	OH5	274	−125	2.19	399	358	0.56
	Sts5	576	−301	1.91	877	775	2.54
	Chimp range	329–1,468	−171 to −727	1.40–3.13	500–2,195	477–1,996	0.81–15.71

[a]Max Prin = maximum principal strain, Min Prin = minimum principal strain, Mode = the absolute value of Max Prin/Min Prin, Max Shear = maximum shear strain, Von Mises = von Mises strain, SED = strain energy density, Chimpanzee data from Smith et al. (in press).
[b]Locations numbered as in Fig. 3.

during premolar biting. This is consistent with the hypothesis that the anterior pillar in *A. africanus* is an adaptation to resist stress during such bites (Rak, 1983; Strait et al., 2009). Such an interpretation may seem counterintuitive insofar as the region containing the stress-reducing trait is not especially strong (if it were, strains would be lower). However, weak regions (with high strains) are precisely those most in need of reinforcement. Natural selection might reasonably be expected to favor anatomical adaptations that strengthen those regions, even though strains remain high in those areas following modification (Strait et al., 2013). This hypothesis could be tested in a modeling experiment in which the anterior pillar was digitally removed from Sts 5. In such a FEM, the hypothesis predicts that strains in the nasal margin will be elevated relative to those found in the unmodified Sts 5 model. Moreover, it will be important to assess strains in the nasal margins of other specimens of *A. africanus* given that facial morphology varies markedly in this species (e.g., Lockwood and Tobias, 1999, 2002).

The use of GM to select specimens preserving a wide range of morphological variability also allowed the detection of variable strain patterns in the zygomatic arches and roots in *P. troglodytes*, even though the strain patterns across the cranium are generally consistent. Most specimens had much higher strains in the arches than in the roots, but two specimens exhibited an opposite pattern. The inverse relationship between arch and root strains in the chimpanzee specimens may relate to the phenomenon in which increasing the structural stiffness of one part of an object may have the effect of elevating strains elsewhere (e.g., Strait et al., 2007).

J_ID: AR Customer A_ID: AR23073 Cadmus Art: AR23073 Ed. Ref. No.: 14-0304 Date: 30-October-14 Stage: Page: 14

TABLE 4. Muscle forces, bite forces, occlusal pressures,[a] and mechanical advantage[b] in the finite element models

Specimen	Total muscle force (N)	P^3 bite force (N)	M^2 bite force (N)	P^3 occlusal area (mm^2)	M^2 occlusal area (mm^2)	P^3 occlusal pressure (MPa)	M^2 occlusal pressure (MPa)	P^3 mechanical advantage	M^2 mechanical advantage
OH 5	5,176	2,053	3,895	185.5	361.2	11.1	10.8	0.40	0.75
Sts 5	2,893	1,178	1,786	118.7	214.2	9.9[c]	8.3[c]	0.41	0.62
PC1−	2,980	1,107	1,522	76.7	105.0	14.4	14.5	0.37	0.51
PC1+	2,540	818	1,251	78.3	118.5	10.4	10.6	0.32	0.49
PC2−	2,536	999	1,481	81.6	96.9	12.2	15.3	0.39	0.58
PC2+	2,408	924	1,350	67.9	84.0	13.6	16.1	0.38	0.56
PC3−	3,268	1,244	1,779	80.5	93.5	15.4	15.8[d]	0.38	0.54
PC3+	3,146	1,310	1,908	79.2	106.7	16.5	17.9	0.42	0.61

[a]Occlusal pressure is calculated as bite force divided by the crown area of the tooth in question (mediodistal length times buccolingual breadth). Tooth dimensions of chimpanzees were measured on CT images, and should be considered approximate. Tooth dimension of fossil hominins were obtained from www.humanoriginsdatabase.org
[b]Mechanical advantage is a measure of biomechanical efficiency, and can be calculated simply as the ratio of the bite force to the total muscle force. In other words, it is equivalent to the ratio of the force outputs to the force inputs.
[c]Note that the tooth crown area data used to calculate pressure are derived from specimen Sts 52a, but that the corresponding bite force data are influenced strongly by the shape and configuration of specimen Sts 5. Thus, the resulting pressure data are heuristic.
[d]Tooth area data were calculated from the better preserved right M^2.

Evaluation of Hypotheses

Strain magnitudes are consistent with the hypothesis (Rak, 1983) that the face of OH 5 is strong and well suited to withstand the loads associated with feeding, at least as implied by static loads applied to the cheek teeth. Moreover the differences in strain distribution observed between OH 5 and both Sts 5 and chimpanzees are consistent with the hypothesis that the anteroposterior position of the zygomatic root is an important factor influencing load resistance in the face (Rak, 1983).

Results were consistent with the hypothesis (Demes and Creel, 1988) that *P. boisei* could efficiently produce high bite forces. Bites on the M^2 in OH 5 did not produce a distractive reaction force at the working-side TMJ even though muscle forces were applied with bilateral symmetry. Given the extraordinary anterior placement of the masseter muscles in this species, it was not obvious that such a finding would be observed. We expect that during normal function, australopiths would have exhibited reductions in balancing-side muscle forces in order to maintain a safety factor serving to reduce the risk of dislocating the working-side TMJ (Spencer, 1999), but our results suggest that there were no special limits on the ability of OH 5 to use its muscles to produce bite force (as would have been implied if it had exhibited a strongly distractive reaction force). This is evidently because the face of OH 5 is so tall that the spatial relationships of the TMJs, teeth, and muscle forces make it easier to maintain a compressive joint force than if the face was short. The triangle of support is not parallel to the tooth row when the TMJ is elevated above the occlusal plane (Spencer, 1995). Indeed, in specimens with a tall face and tall mandibular ramus, bites on the molars can produce a triangle of support that is very steeply inclined. Likewise, the muscle resultant is not simply vertical, but can be inclined, especially in species like *P. boisei* in which the masseter origin is positioned far anteriorly but the masseter insertion is positioned relatively posteriorly. Thus, in *P. boisei* it is more correct to state that the masseter muscle is strongly inclined rather than to describe it as having shifted anteriorly. Because both the triangle of support and the muscle resultant are inclined (but not necessarily perpendicular to each other), it is theoretically possible to keep the resultant within the triangle during molar bites despite the anterior placement of the masseter origin (Spencer, 1995), and this evidently occurs in *P. boisei*. It is biomechanically difficult to configure the feeding apparatus so as to allow a primate to generate high bite forces across the whole length of a mesiodistally long cheek tooth row, and yet the highly derived facial morphology of *P. boisei* appears to meet that challenge. There is no reason to reject a hard-object feeding hypothesis on these grounds.

Occlusal pressures in OH 5 were at the bottom end of the range seen in chimpanzees and well below the chimpanzee mean. Occlusal pressures in Sts 5 fell below the chimpanzee range of variation. These results suggest that australopith adaptations for increasing bite force cannot be explained fully by the need to maintain occlusal pressures on expanded tooth surfaces (Walker, 1981). Pressure across the entire occlusal surface is a relevant performance metric when feeding on compliant foods that spread over a tooth, but hard foods contact teeth across a much smaller area (even when biting on many small, hard objects at once), so the high bite forces in *P. boisei* could have generated enormous stresses in such items (Demes and Creel, 1988).

Other Estimates of Bite Force in OH 5

As described in Table 4, bite forces at the P^3 and M^2 in OH 5 greatly exceed those of Sts 5 and all six chimpanzees when the models are loaded with isometrically scaled, bilaterally symmetrical muscle forces simulating a maximal bite. These results conform well to those of Eng et al. (2013). However, they also exceed those obtained in a prior simulation (Wroe et al., 2010) of biting in OH 5, and that discrepancy warrants discussion.

Wroe et al. (2010) used FEA to examine bite force production in humans, extant non-human hominoids, and

ID: chandrasekar.v Time: 20:56 I Path: N:/3b2/AR##/Vol00000/140193/APPFile/JW-AR##140193

J_ID: AR Customer A_ID: AR23073 Cadmus Art: AR23073 Ed. Ref. No.: 14-0304 Date: 30-October-14 Stage: Page: 15

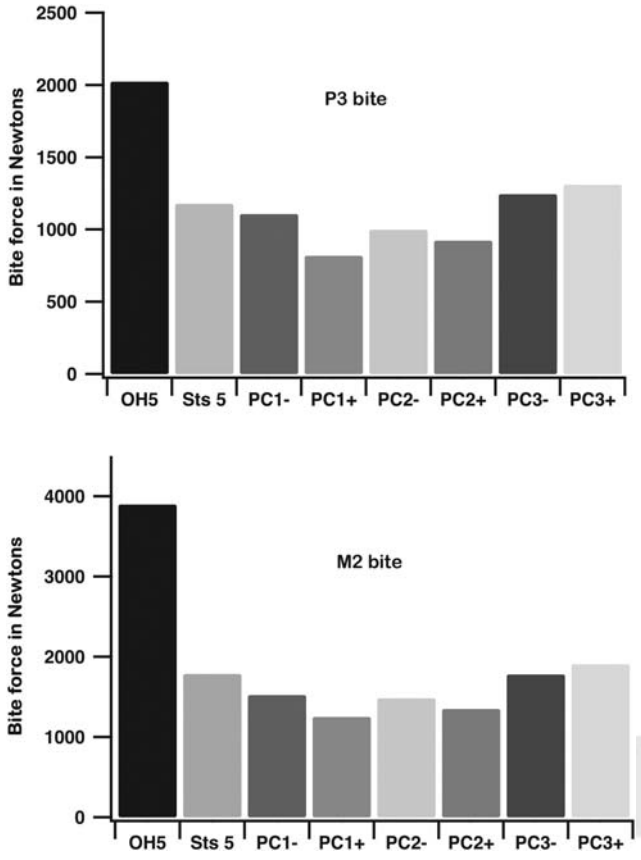

Fig. 8. Bite force. Bite force calculated during FEA of the crania of *P. boisei, A. africanus*, and *P. troglodytes*. Bites were simulated on the P^3 and M^2 using muscle forces that were scaled to the 2/3rd power of model bone volume.

some fossil hominins, including OH 5. Their key finding was that modern humans are able to generate and withstand higher bite forces than anticipated, but they also presented bite force data for the other species. They do not discuss OH 5 or chimpanzees extensively, but they present data for these taxa that can be compared to the results obtained by us.

Results obtained by Wroe et al. (2010) for chimpanzees are fully compatible with ours. They report an M2 bite force of 1,511 N, which falls within the range of values obtained by us, 1,251–1,908 N. Moreover, the total muscle force input into their chimpanzee model (2,682.6 N) is also within our range (2,408–3,268 N). From their data, it is possible to calculate a mechanical advantage of 0.56 that once again falls within our range (0.49–0.61).

Results from OH 5 differ considerably between the two studies. Wroe et al. (2010) obtained a maximum M^2 bite force of 2,161 N, while we obtained 3,895 N. Thus, our bite force observation is 80% greater than theirs. Muscle force inputs seem unlikely to fully explain this discrepancy. Wroe et al. (2010) applied a total muscle force of 4,430.4 N, compared to the 5,176 N in our model. Our force value is therefore only 17% greater than theirs, and in any case neither study can claim to model muscle forces in *P. boisei* with great accuracy; the forces applied to both models are coarse estimates. The two studies distributed their muscle force vectors in slightly different ways. We modeled distinct muscle compartments (i.e., superficial masseter, deep masseter, and anterior temporalis), while Wroe et al. (2010) modeled whole muscles without discriminating among muscle compartments (i.e., masseter, temporalis). Wroe et al. (2010) also modeled the forces as trusses originating and inserting on multiple points, while we modeled them as a "fan" of vectors wrapping around bone surfaces converging on a point. These differences undoubtedly lead to differences in the leverages of individual muscle force vectors. One possibility worth investigating would be to determine if any trusses in Wroe et al.'s (2010) OH 5 model pass inferior to the TMJs as they pass from origin to insertion. Trusses representing the posterior temporalis might be at risk of doing so. If so, then those trusses would produce torques that oppose those of the other trusses representing the rest of the temporalis muscle, and would artificially reduce bite forces. In contrast to Wroe et al. (2010), the posterior temporalis is not modeled in the present study, so these modeling differences might partially explain the discrepancy in bite force between the two studies. However, if all trusses in Wroe et al. (2010) pass superior or anterior to the TMJs, then the proposed explanation would be invalid. A simple way of testing this explanation would be to de-activate the truss representing the inferior-most fibers of posterior temporalis in the Wroe et al. (2010) OH 5 model. If the resulting bite force increases despite the fact that total muscle force input has decreased, then the line of action of the de-activated truss passes below the TMJs and the explanation is credible. Regardless, it is probable that the source of the discrepancy concerns decisions about the modeling of muscle forces, because the mechanical advantage found by Wroe et al. (2010) is far less (0.49) than that obtained by us (0.75). Indeed, the value obtained by them for OH 5 is less than that of their chimpanzee and all but one of our chimpanzees. Considering that the masseter origin is placed farther anteriorly in OH 5 than in any chimpanzee, and that the moment arm of a molar bite point in OH 5 is not obviously elongated (e.g., Demes and Creel, 1985), the findings of Wroe et al. (2010) appear to conflict with expectations based on jaw lever biomechanics. In contrast, we believe that our results are compatible with those expectations and with earlier estimates of jaw leverage (Demes and Creel, 1988). However, a close comparison of our models and those of Wroe et al. (2010) are needed in order to isolate the source of the discrepancy between the results of the two studies.

Implications for Feeding Ecology

Our results are consistent with the hypothesis that the cranium of *P. boisei* is strong when subjected to feeding loads and configured to efficiently produce a high bite force distributed along a mesiodistally long postcanine tooth row. It is evident that the feeding apparatus of *P. boisei* had considerable biomechanical capability, and possessed some performance advantages relative to chimpanzees and other australopiths. Simultaneously, the craniodental morphology of this species (and robust australopiths, in general) is highly derived (e.g., Rak, 1983; Strait and Grine, 2004). It is reasonable to infer, therefore, that the configuration of the facial skeleton of

TABLE 5. Mechanical and material properties of African grass and sedge seeds[a]

Species[b]	Extent of 'shell' tissue examined	Location	Length (mm)	Width (mm)	Thickness (mm)	Moisture content (%dry wt)	Pericarp E_r (GPa)	Pericarp H (MPa)	Seed Coat E (GPa)	Seed Coat H (MPa)
Sporobolus spicatus	Pericarp: 5 areas scanned (N = 111); Seed coat: 7 areas scanned (N = 123)	Lake Manyara Nat. Park	2.01 (0.10) N = 10	0.49 (0.08) N = 10	0.33 (0.08) N = 6	6.15	1.82 (0.65); Range, 1.01–3.60	111 (43); Range, 60–264	2.98 (1.20); Range, 1.61–5.84	125 (43); Range 65–236
Sporobolus ioclados	Pericarp: 3 areas scanned (N = 20); Seed coat:3 areas scanned (N = 48)	Ngorongoro Crater	2.57 (0.10) N = 10	0.76 (0.08) N = *10*	0.49 (0.04) N = *10*	9.04	4.08 (1.27); Range, 2.78–7.53	293 (143); Range, 150–743	4.70 (2.24); Range, 2.32–10.61	248 (182); Range 194–828
Carex monostachya	Pericarp: 5 areas scanned (N = 68); Seed coat: 9 areas scanned (N = 77)	Arusha Nat. Park (Meru Mts.)	3.12 (0.25)* N = 10	1.16 (0.14)* N = 10	0.87 (0.09)* N = 5	6.96	6.28 (2.17); Range, 2.83–10.81	585 (323); Range, 185–1529	6.19 (1.45); Range, 3.73–9.03	254 (100); Range 143–498
Cyperus bulbosus	Pericarp: 3 areas scanned (N = 93); Seed coat: 4 areas scanned (N = 157)	Mayi ya chai, Usa river, Arusha	1.15 (0.09) N = 10	0.71 (0.10) N = 10	0.52 (0.09) N = 5	5.84	0.458 (0.122); Range, 0.21–0.82	76 (27); Range, 31–146	3.55 (1.94); Range, 0.85–9.37	162 (66); Range 72–374
Pennisetum stramineum	Pericarp: 5 areas scanned (N = 40); Seed coat: 4 areas scanned (N = 163)	Escarpment Rift Valley Lake Manyara Nat. Park	3.62 (0.37) N = 11	1.05 (0.13) N = 11	0.83 (0.13) N = 5	6.49	7.03 (3.51); Range, 2.16–15.15	558 (459); Range, 138–1697	4.48 (0.984); Range, 1.79–8.36	179 (54); Range 85–342
Cynodon dactylon	Pericarp: 5 areas scanned (N = 94); Seed coat: 4 areas scanned (N = 82)	Arusha Town TPR1 nr. Nat. Herbarium	2.49 (0.19) N = 12	0.93 (0.07) N = 12	0.33 (0.07) N = 5	6.15	2.49 (1.42); Range, 0.49–6.16	173 (106); Range, 28–427	3.18 (1.69); Range, 1.69–8.25	174 (99); Range 50–538

TABLE 5. (continued).

Species[b]	Extent of 'shell' tissue examined	Location	Length (mm)	Width (mm)	Thickness (mm)	Moisture content (%dry wt)	Pericarp E_r (GPa)	Pericarp H (MPa)	Seed Coat E (GPa)	Seed Coat H (MPa)
Eragrostis sp.	Pericarp: 5 areas scanned (N = 82); Seed coat: 4 areas scanned (N = 40)	Meru Mts.	1.40 (0.18) N = 10	0.63 (0.08) N = 10	0.46 (0.05) N = 5	6.14	1.86 (0.542); Range, 1.09–3.14	184 (65); Range, 76–321	3.71 (1.89); Range, 1.08–7.66	256 (228); Range 45–826

[a]All data are means (std. dev.); N = number of samples tested; *bare seed measurement only. E = elastic modulus. H = hardness.
[b]All species utilize the C4 photosynthetic pathway except for *Carex monostachya* (e.g., Hesla et al., 1982; Prendergast et al., 1986; Christin et al., 2009; Sage et al., 2011).

this species (or the last common ancestor of a robust australopith clade) represents a feeding adaptation of some kind. Which foods provided the selection pressure that led to the evolution of these adaptations? There is no single method of analysis that can fully answer this question (Strait et al., 2013). Rather, a synthesis of multiple lines of evidence is needed in order to discern which food item or items may be driving the evolution of this morphology.

Foods can be hard or compliant/tough (Lucas et al., 2000), and can be large or small. Compliant/tough foods deform considerably under load, frustrating fracture unless sharp crested teeth can push cracks through them to produce fragmentation (Lucas et al., 2000). It has been suggested that compliant/tough foods like sedge pith and grass blades were frequently consumed by *P. boisei* and that the robust face and large chewing muscles of this species are adaptations for producing and withstanding highly repetitive feeding loads (Van der Merwe et al., 2008; Cerling et al., 2011a). There is little doubt that *P. boisei* was capable of feeding in this manner, but even if it is true that compliant/tough foods were eaten regularly by this species, it seems implausible that its facial skeleton evolved adaptations for feeding on these foods while its blunt occlusal morphology simultaneously became maladapted to consume such items (Strait et al., 2013). Thus, the selective importance of compliant/tough foods was evidently low regardless of the frequency with which they were eaten. It is more plausible to infer that the consumption of hard foods provided a meaningful selection pressure contributing to the evolution of the feeding apparatus in *P. boisei* (and, arguably, at least some other hominins), and all of the biomechanical results observed here are consistent with this scenario. Note that our interpretation depends critically on a traditional understanding of the functional significance of occlusal morphology (e.g., Lucas et al., 1985). In contrast, if it can be shown that blunt teeth with low occlusal relief are efficient at processing compliant/tough foods, then this interpretation would be weakened.

Blunt cheek teeth with thick enamel are well suited for consuming hard foods like nuts and seeds because such teeth are less likely to fail under the high loads needed to fracture the food item (Lucas et al., 2008; Constantino et al., 2010). Large nuts and seeds must be ingestively processed in order to access the seed kernel, but the incisors and canines of *P. boisei* are small and more susceptible to fracture than its massive premolars (Constantino et al., 2010), on which nut ingestion is likely to have occurred. The facial skeleton of *P. boisei* is well designed to resist premolar loads, but species that are specialized to bite forcefully on their premolars are not expected to have distally positioned molar teeth (Greaves, 1978; Spencer, 1999). Rather, the face of *P. boisei* is biomechanically suited to generate and resist high or repetitive bite forces on both the molars and premolars. Whereas large, hard items would have been fractured on the premolars, smaller hard items would have been fractured on the molars or processed in bulk across the entire postcanine tooth row (Lucas et al., 1985). Likely candidates for such small, hard items are the seeds of African grasses and sedges, although the material properties of these grains have not previously been well documented. Accordingly, we performed mechanical

J_ID: **AR** Customer A_ID: **AR23073** Cadmus Art: **AR23073** Ed. Ref. No.: **14-0304** Date: **30-October-14** Stage: Page: **18**

TABLE 6. Pairwise comparisons using Pillai's Trace (following MANOVA) between primate species using four dental microwear texture variables (*Asfc, epLsar, Tfv, HAsfc81*)

	Ap	Ab	Ah	Cn	C	Cx	Ca	Cg	Cp	Gb	Gg	La	Mf	Pt	Pc	Pu	Pp	Pr	Pb	Se	Tg	Tc
Alouatta palliata	–																					
Ateles belzebuth	**	–																				
Ateles hybridus	NS	ns	–																			
Cebus nigrittus rob.[a]	***	*	*	–																		
Cebus sp.[a]	NS	**	*	*	–																	
Cebus xanthosternos[a]	NS	NS	*	ns	ns	–																
Cercocebus atys	****	NS	*	ns	ns	ns	–															
Colobus guereza	***	*	*	****	NS	NS	****	–														
Colobus polykomos	****	NS	NS	*	*	ns	*	***	–													
Gorilla beringei	****	NS	*	NS	NS	NS	**	ns	Ns	–												
Gorilla gorilla	****	NS	NS	****	***	NS	NS	ns	Ns	ns	–											
Lophocebus albigena	****	**	**	ns	ns	ns	ns	****	*	NS	NS	–										
Macaca fascicularis	****	*	**	NS	NS	NS	NS	**	NS	NS	NS	NS	–									
Pan troglodytes	****	ns	*	*	*	*	*	**	**	NS	NS	*	ns	–								
Papio cynocephalus	****	**	ns	****	**	ns	ns	**	*	ns	*	ns	ns	ns	–							
Papio ursinus	****	ns	ns	**	ns	ns	ns	****	*	ns	ns	ns	ns	*	***	–						
Pongo pygmaeus	*	NS	NS	*	*	ns	*	NS	Ns	NS	NS	ns	**	NS	ns	**	–					
Presbytis rubicunda	ns	ns	ns	***	**	ns	ns	*	*	ns	ns	ns	***	**	***	****	ns	–				
Procolobus badius	****	ns	ns	***	***	ns	ns	**	Ns	ns	ns	ns	ns	*	*	*	ns	ns	–			
Semnopithecus entellus	ns	*	*	****	****	*	ns	ns	Ns	ns	ns	ns	**	**	ns	**	ns	**	**	–		
Theropithecus gelada	ns	***	****	****	**	*	*	**	*	*	**	NS	NS	***	****	****	***	****	**	ns	–	
Trachypithecus cristatus	ns	NS	*	**	**	NS	*	ns	Ns	ns	**	NS	***	***	****	****	NS	ns	ns	ns	**	–

The large number of comparisons complicates efforts to identify significant differences. "*" refers to comparisons significant at the $P < 0.05$ level, "**" at the $P < 0.01$ level, "***" at the $P < 0.001$ level, and "****" at the Bonferroni protected probability level of $P < 0.000216$. "NS" and "ns" refer to a comparison that is not significant at any of those levels, but "NS" refers to pairs of species that do not differ from each other at any level of significance *despite* marked differences in diet. Species names are abbreviated along the top row. Data from Scott et al. (2012).

[a]We do not fully agree with the species-level taxonomic attributions of the *Cebus* specimens in the Scott et al. (2012), but we employ their groupings here.

tests on seeds gathered from African habitats (see Appendix) and found that their indentation hardness and material stiffness (i.e., elastic modulus) (Table 5) are broadly comparable to those of much larger nut and seed shells (Lucas et al., 2009, 2012). Grass seed consumption would entail highly repetitive loading, because the seeds are individually so small that many would need to be eaten in order to provide a meaningful source of nutrition. Many African grasses and sedges employ the C4 photosynthetic pathway (e.g., Hesla et al., 1982; Prendergast et al., 1986; Christin et al., 2009; Sage et al., 2011), and thus their consumption would be compatible with the stable carbon isotope signature of *P. boisei* (Van der Merwe et al., 2008; Cerling et al., 2011a).

Another category of small, hard food items include the corms and bulbs of various African plants (Dominy et al., 2008). Recent studies (Yeakel et al., 2013; Macho, 2014) suggest that such underground storage organs may have figured prominently in the diet of *P. boisei*, and the regular or fallback consumption of these foods is consistent with our hypothesis. However, it is worth bearing in mind that the mechanical properties of hard foods vary considerably and thus pose different challenges to the hominins consuming them. For example, the material stiffness (as measured by the elastic modulus) of corms and bulbs (Dominy et al., 2008) is roughly three orders of magnitude less than that of seed and nut shells (Table 5; Lucas et al., 2009, 2012). Thus, corms and bulbs are about as hard as seed kernels, not seed coats. It is therefore worth asking whether or not natural selection would favor the evolution of the extraordinary feeding apparatus of *P. boisei* in order to consume such foods. In this regard, experimental studies on living primates are needed that document and compare the bite forces, bone strains, and number of chewing cycles associated with eating/processing grains (both individually and by the mouthful), corms, bulbs, and large seeds with intact shells.

Our interpretation is inconsistent with dental microwear analyses that seemingly do not preserve evidence of hard object feeding in *P. boisei* (Ungar et al., 2008; see also Cerling et al., 2011a). Rather, microwear textures in this species resemble those of folivorous primates, although microwear features are less consistently aligned in *P. boisei* than in certain extant folivores. However, statistical analysis of primate dental microwear texture data (Scott et al., 2012) reveals that these data do not consistently discriminate among species with different diets. Although some primate species can be discriminated in this fashion (Scott et al., 2012), pairwise comparisons between primate taxa based on MANOVA of rank-ordered data reveal that many pairs of species do not differ significantly in their multivariate microwear patterns (Table 6) despite evident differences in diet (Scott et al., 2012). For example, there are a number of statistically non-significant differences between: (1)

ID: **chandrasekar.v** Time: 20:57 I Path: N:/3b2/AR##/Vol00000/140193/APPFile/JW-AR##140193

J_ID: AR Customer A_ID: AR23073 Cadmus Art: AR23073 Ed. Ref. No.: 14-0304 Date: 30-October-14 Stage: Page: 19

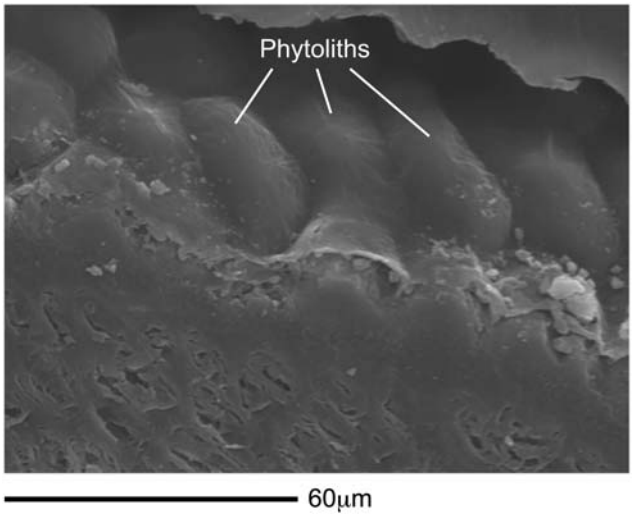

Fig. 9. Phytoliths on seed. Scanning electron micrograph of the pericarp of a sedge seed, *Cyperus bulbosus*. Energy dispersive spectroscopy reveals that the rounded, pod-like structures on the cell wall of the pericarp are densely packed phytoliths (Supporting Information Fig. A2). The flat, sectioned face of the seed is below the phytoliths.

several of the relatively folivorous and/or seed eating colobines and the relatively frugivorous atelines; (2) the relatively folivorous *Gorilla* species and most of the various hard-object feeding species in *Cebus, Lophocebus, Pongo*, and *Cercocebus*, as well as most of the soft fruit eaters in *Ateles, Pan* and *Macaca*; (3) any of the great apes, whose diets range from folivory to frugivory to hard-object feeding; (4) the highly folivorous *Colobus guereza* and *Trachypithecus cristatus* and some of the hard object feeders in *Cebus, Lophocebus*, and *Pongo*; (5) the grass eating *Theropithecus* and both the hard-object feeding *Lophocebus* and the soft fruit eating *Macaca*; and (6) the frugivorous *Ateles* and some of the destructive foragers in *Cebus*. Thus, multivariate statistical analysis of the most comprehensive microwear data set collected to date (Scott et al., 2012) does not consistently support the notion that microwear signals reliably sort primates according to dietary category. Univariate analyses of these data yield similar results (Strait et al., 2013).

Moreover, nanowear experiments suggest that microwear formation is governed strongly by the geometry and material properties of abrasive particles rather than foods (Lucas et al., 2013). Nanoindentation tests (Table 5) indicate that the outer pericarps of East African grass and sedge seeds are much less hard than dental enamel (Lucas et al., 2013). Seed shells (including those of large nuts) and other plant tissues are therefore too soft to be an important source of abrasive dental microwear, but phytoliths ingested along with grass and sedge seeds (Piperno, 2006) are likely to induce light non-abrasive microgrooves on tooth occlusal surfaces (Lucas et al., 2013). Notably, all of the grass and sedge seeds examined by us contain phytoliths, and some seeds are so densely coated with them that it is as if the seeds are armored (Fig. 9). Thus, seasonal grass or sedge seed consumption (Jolly, 1970) is compatible with what is currently known about the biomechanics, dental microwear, and isotopic signature of *P. boisei* (Van der Merwe et al., 2008; Ungar et al., 2008; Cerling et al., 2011a; Ungar and Sponheimer, 2011), and the rare consumption of larger nuts and seeds from woody plants cannot be ruled out.

A recent study (Rabenold and Pearson, 2011) has demonstrated a correlation between phytolith consumption and relative enamel thickness in extant primates, and on that basis suggested that enhanced enamel thickness evolved in *P. boisei* as an adaptation to extend tooth life in the face of phytolith-induced tooth wear. We agree that *P. boisei* may have consumed a diet high in phytoliths, that thick enamel extends tooth life against abrasive wear, and that *P. boisei* exhibits impressive macroscopic wear. However, the proposed causal link between phytolith consumption and macroscopic wear (Rabenold and Pearson, 2011) is based on the premise that phytoliths are sufficiently hard as to abrade enamel. Recently collected data suggest that this is not the case (Lucas et al., 2013). Rather, phytoliths are softer than enamel and although they can mark tooth surfaces by rearranging enamel crystals through a process known as "rubbing" (in which the phytolith and tooth surface mutually deform), they lack the hardness necessary to create rigid-plastic contacts that would result directly in the loss of enamel volume from the tooth crown. In principle, repeated rubbing could weaken the enamel crystals on the occlusal surface leading eventually to wear (loss of volume), but this process should be slower than direct abrasion caused by a hard, angular particle. How much slower is presently unknown, but *P. boisei* evidently wore its teeth quickly (e.g., the M^1 of OH 5 wore down to the dentin before the M^3 came into full occlusion). Thus, phytolith consumption seems unlikely to be a major source of macroscopic wear in *P. boisei*, and is similarly unlikely to explain the evolution of thick enamel in this species and other australopiths.

If phytolith consumption does not explain macrosopic wear patterns in *P. boisei*, then what does? If the fine microgrooves seen on *P. boisei* teeth are a result of abrasive scratching, then sedimentary grit derived either from soils or wind-born particles such as quartz dust (Lucas et al., 2013) or, when present, volcanic ash (e.g., Strömburg et al., 2013) seem to be likely wear agents. Underground storage organs would reasonably be expected to introduce grit into the oral cavity, although Dominy (2012) notes that corms have tunics that can be peeled to remove sediments. Clearly, more work is needed to document the incidence, geometry, and material properties of abrasive particles adhering to East African plant foods. On the other hand, if the microwear features seen in *P. boisei* constitute rubbing marks, then it seems likely that microwear patterns are unrelated to macrowear patterns in this species. Rather, the macroscopic wear may have been caused either by extensive tooth-on-tooth contact, or by grit whose abrasive scratches have been obscured by subsequent rubbing marks associated with a high-phytolith diet (Lucas et al., 2013).

In theory, nanoscale microscopy ought to be able to discern whether individual microwear features were caused by rubbing or abrasion (Lucas et al., 2013). Rubbing, as when a phytolith contacts a tooth, should result

ID: chandrasekar.v Time: 20:57 I Path: N:/3b2/AR##/Vol00000/140193/APPFile/JW-AR##140193

in a mark that is smoothly curved in cross-section and bounded by raised blunt ridges (prows) formed as the enamel crystals are displaced. In contrast, abrasive marks should be sharply angular in cross-section and should not show evidence of prowing. *In vivo* experimental tests are needed to determine whether or not abrasive vs. rubbing marks can be consistently discriminated from each other in mammalian microwear fabrics and, if so, a research priority should be an assessment of the nature of microwear features in *P. boisei*.

Our interpretation that hard foods were a selectively important component of the diet of *P. boisei* is consistent with phylogenetic patterns. *P. boisei* is functionally and ecomorphologically similar to *P. robustus* from southern Africa, and these species are either close relatives in a *Paranthropus* clade (e.g., Strait and Grine, 2004) or they are polyphyletic and independently descended from distinct eastern and southern African gracile australopiths (e.g., Walker et al., 1986). At present, there is a general agreement that *P. robustus* is likely to have consumed hard-objects (e.g., Grine and Kay, 1988; Teaford and Ungar, 2000; Scott et al., 2005; Ungar et al., 2008; Strait et al., 2013). If, as we suggest, robust morphology represents an adaptation to feeding on such foods, then either robust morphology evolved at the base of the *Paranthropus* clade as an adaptation to consume such a diet, or it evolved convergently in two distinct lineages as a result of common selection pressures caused by eating similar foods. Both scenarios seem plausible. In contrast, if *P. boisei* is adapted to consume compliant/tough foods, then either adaptations for feeding on such items evolved at the base of the *Paranthropus* clade and happened to produce a morphology that was equally well or even better suited to feeding on hard foods (as in *P. robustus*), or *P. boisei* and *P. robustus* independently converged on a *common* morphology in response to feeding on different types of food (Strait et al., 2013). We are not aware of any comparable examples of such evolutionary scenarios in primates.

The appearance of robust morphology coincides roughly with complex changes in the vegetation of Early Pleistocene East African habitats. These changes have been characterized as an expansion of grasslands and a concomitant reduction in woody vegetation associated with the appearance of grazing bovid species (e.g., Bobe, 2011; Cerling et al., 2011b), although recent work suggests instead that grasslands declined while xeric shrublands expanded during this time period (Feakins et al., 2013). Regardless, enhanced foraging opportunities in expanding habitats might have been complemented by the need to more effectively exploit resources in shrinking habitats. Robust morphology can be seen as an adaptation for better accessing hard foods in all contexts. These new ecological conditions were evidently unfavorable for gracile australopith populations, since in any given region none survive long after *Homo* and *Paranthropus* appear. Yet, gracile australopiths were almost certainly the ancestors of both genera. This implies indirectly that the evolution of *Homo* and *Paranthropus* should not be considered distinct events but rather two outcomes of one event, the disruption of gracile australopith niches. The evolutionary trajectory of *Paranthropus* suggests that food-processing behavior was a component of the niche that was disturbed in significant ways. Some gracile populations may have adopted an alternative strategy for coping with these disturbances, leading eventually to the evolution of *Homo*.

CONCLUSION

Several hypotheses concerning the biomechanics of feeding in *P. boisei* were tested using FEA informed by GM. Results indicate that OH 5 could have efficiently generated high bite forces at multiple locations along the cheek tooth row, and that the facial skeleton was well suited to withstand those loads. A synthesis of multiple lines of evidence suggests that the consumption of hard foods may have been an important selective pressure influencing the evolution of australopith cranial form. An understanding of evolutionary trends in *Paranthropus* may inform our understanding of trends that led to the evolution of *Homo* insofar as trends in the former provide information about the selection pressures affecting the common ancestor of both groups.

ACKNOWLEDGEMENTS

Authors thank Siobhan Cooke and Claire Terhune for the opportunity to contribute to this special issue, and to participate in the symposium on which it was based. This article benefitted from insightful comments by Laurie Godfrey, Betsy Dumont, Kornelius Kupczik, and anonymous reviewers. Adam Gordon provided welcome statistical advice. Frank Mbago gathered grass seeds growing wild in Tanzania. Authors thank staff at the National Museum of Tanzania, the Transvaal Museum, the Kuwait University Nanotechnology Research Facility, the Herbarium of the University of Dar es Salaam, the Senckenberg Research Foundation, the Lincoln Park Zoo, the Yerkes Primate Research Center (YPRC; NIH Base Grant RR00165), and the Southwest National Primate Research Center (SNPRC; NIH-NCRR grant P51 RR013986). Jerilyn Pecotte and Kelly Clark of SNPRC and Kay Lee Summerville of YPRC kindly arranged shipping and processing of primate biological materials. Finite element models are available for download at www.biomesh.org

AUTHOR CONTRIBUTIONS

All authors contributed to the interpretation of the data presented in this paper and the writing of the document. D.S.S., G.W.W, M.A.S., P.W.L., P.C.D, I.R.G., C.F.R., B.G.R., B.W.W., Q.W. and D.E.S. conceived of the project. S.B. and G.W.W. produced the virtual reconstruction of OH 5. A.L.S., K.T., J.A.L., L.C.P.S. built finite element models and collected corresponding strain data. A.L.S. and P.C.D. collected *ex vivo* strain data. P.W.L., S.M., A.v.C., K.A.-F., and A.S. collected data on the mechanical properties of grass seed. P.C.D. and L.C.P.S. collected data on the material properties of craniofacial bone in apes.

LITERATURE CITED

Benazzi S, Bookstein FL, Strait DS, Weber GW. 2011. A new OH5 reconstruction with an assessment of its uncertainty. J Hum Evol 61:75–88.

Benazzi S, Kullmer O, Schultz D, Gruppioni G, Weber GW. 2013. Individual tooth macrowear pattern guides the reconstruction of

Sts 52 (*A. africanus*) dental arch. Am J Phys Anthropol 150:324–329.

Bobe R. 2011. Fossil mammals and paleoenvironments in the Omo-Turkana Basin. Evol Anthropol 20:254–263.

Cerling TE, Mbua E, Kirera FM, Manthi FK, Grine FE, Leakey MG, Sponheimer M, Uno KT. 2011a. Diet of *Paranthropus boisei* in the early Pleistocene of East Africa. Proc Natl Acad Sci USA 108:9337–9341.

Cerling TE, Wynn JG, Andanje SA, Bird MI, Korir DK, Levin NE, Mace W, Macharia AN, Quade J, Remien CH. 2011b. Woody cover and hominin environments in the past 6 million years. Nature 476:51–56.

Christin PA, Salamin N, Kellogg EA, Vicentini A, Besnard G. 2009. Integrating phylogeny into studies of C4 variation in the grasses. Plant Physiol 149:82–97.

Clausen P, Wroe S, McHenry C, Moreno K, Bourke J. 2008. The vector of jaw muscle force as determined by computer-generated three dimensional simulation: a test of Greaves' model. J Biomech 41:3184–3188.

Constantino PJ, Lee JJ-W, Chai H, Zipfel B, Ziscovicic C, Lawn BR, Lucas PW. 2010. Tooth chipping can reveal the diet and bite forces of fossil hominins. Biol Lett 6:826–829.

Davis JL, Dumont ER, Strait DS, Grosse IR. 2011. An efficient method of modeling material properties using a thermal diffusion analogy: an example based on craniofacial bone. PLoS One 6: e17004.

Demes B, Creel N. 1988. Bite force, diet, and cranial morphology of fossil hominids. J Hum Evol 17:657–670.

Dominy NJ. 2012. Hominins living on the sedge. Proc Natl Acad Sci USA 109:20171–20172.

Dominy NJ, Vogel ER, Yeakel JD, Constantino P, Lucas PW. 2008. Mechanical properties of plant underground storage organs and implications for dietary models of early hominins. Evol Biol 35: 159–175.

Dumont ER, Davis JL, Grosse IR, Burrows AM. 2011a. Finite element analysis of performance in the skulls of marmosets and tamarins. J Anat 218:151–162.

Dumont ER, Grosse IR, Slater GJ. 2009. Requirements for comparing the performance of finite element models of biological structures. J Theor Biol 256:96–103.

Dumont ER, Ryan TM, Godfrey LR. 2011b. The *Hadropithecus* conundrum reconsidered, with implications for interpreting diet in fossil hominins. Proc R Soc B 278:3654–3661.

Eng CM, Lieberman DE, Zink KD, Peters MA. 2013. Bite force and occlusal stress production in hominin evolution. Am J Phys Anthropol 151:544–557.

Feakins SJ, Levin NE, Liddy HM, Sieracki A, Eglinton TI, Bonnefille R. 2013. Northeast African vegetation change of 12 m.y. Geology 42:295–298.

Greaves WS. 1978. The jaw lever system in ungulates: a new model. J Zool Lond 184:271–285.

Grine FE, Kay RF. 1988. Early hominid diets from quantitative image analysis of dental microwear. Nature 333:765–768.

Grosse IR, Dumont ER, Coletta C, Tolleson A. 2007. Techniques for modeling muscle-induced forces on finite element models of skeletal structures. Anat Rec A 290:1069–1088.

Hesla ABI, Tieszen LL, Imbamba SK. 1982. A systematic survey of C3 and C4 photosynthesis in the Cyperaceae of Kenya, East Africa. Photosynthetica 16:196–205.

Hylander WL. 1979. Mandibular function in *Galago crassicaudatus* and *Macaca fascicularis*: an *in vivo* approach to stress analysis of the mandible. J Morph 159:253–296.

Hylander WL, Johnson KR. 1997. *In vivo* bone strain patterns in the zygomatic arch of macaques and the significance of these patterns for functional interpretations of craniofacial form. Am J Phys Anthropol 120:203–232.

Hylander WL, Picq PG, Johnson KR. 1991. Masticatory-stress hypotheses and the supraorbital region of primates. Am J Phys Anthropol 86:1–36.

Hylander WL, Ravosa MJ, Ross CF. 2004. Jaw muscle recruitment patterns during mastication in anthropoids and prosimians. In: Anapol F, German RZ, Jablonski NJ, editors. Shaping primate evolution. Cambridge: Cambridge University Press. p 229–257.

Hylander WL, Ravosa MJ, Ross CF, Wall CE. 1998. Mandibular corpus strain in primates: further evidence for a functional link between symphyseal fusion and jaw-adductor muscle force. Am J Phys Anthropol 107:257–271.

Jolly CJ. 1970. The seed-eaters: a new model of hominid differentiation based on a baboon analogy. Man 5:5–26.

Kupczik K, Dobson CA, Crompton RH, Phillips R, Oxnard CE, Fagan MJ, O'Higgins P. 2009. Masticatory loading and bone adaptation in the supraorbital torus of developing macaques. Am J Phys Anthropol 139:193–203.

Kupczik K, Dobson CA, Fagan MJ, Crompton RH, Oxnard CE, O'Higgins P. 2007. Assessing mechanical function of the zygomatic region in macaques: validation and sensitivity testing of finite element models. J Anat 210:41–53.

Lockwood CA, Tobias PV. 1999. A large male hominin cranium from Sterkfontein, South Africa, and the status of *Australopithecus africanus*. J Hum Evol 36:637–685.

Lockwood CA, Tobias PV. 2002. Morphology and affinities of new hominin cranial remains from Member 4 of the Sterkfontein Formation, Gauteng Province, South Africa. J Hum Evol 42:389–450.

Lucas PW, Constantino P, Wood B, Lawn B. 2008. Dental enamel as a dietary indicator in mammals. BioEssays 30:374–385.

Lucas PW, Corlett RT, Luke DA. 1985. Plio-pleistocene hominid diets: an approach combining masticatory and ecological analysis. J Hum Evol 14:187–202.

Lucas PW, Gaskins JT, Lowrey TF, Harrison ME, Morrogh-Bernard H, Cheyne SM, Begley MR. 2012. Evolutionary optimization of material properties of a tropical seed. J Roy Soc Interface 9:34–42.

Lucas PW, Omar R, Al-Fadhalah K, Almusallan AS, Henry AG, Michael S, Thai LA, Wtzke J, Strait DS, Atkins AG. 2013. Mechanisms and causes of wear in tooth enamel: implications for hominin diets. J Roy Soc Interface 10:20120923.

Lucas PW, Turner IM, Dominy NJ, Yamashita N. 2000. Mechanical defenses to herbivory. Ann Bot 86:913–920.

Macho GA. 2014. Baboon feeding ecology informs the dietary niche of *Paranthropus boisei*. PLoS ONE9:e84942.

McNulty KP, Frost SR, Strait DS. 2006. Examining affinities of the Taung child by developmental simulation. J Hum Evol 51:274–296. AQ3

Mitteroecker P, Gunz P, Bernhard M, Schaefer K, Bookstein FL. 2004. Comparison of cranial ontogenetic trajectories. J Hum Evol 46:679–698.

Nakashige M, Smith AL, Strait DS. 2011. Biomechanics of the anthropoid postorbital septum investigated using finite element analysis. J Anat 218:142–150.

O'Higgins P, Cobb SN, Fitton LC, Gröning F, Phillips R, Liu J, Fagan MJ. 2011. Combining geometric morphometrics and functional simulation: an emerging toolkit for virtual functional analyses. J Anat 218:3–15.

O'Higgins P, Jones N. 1998. Facial growth in *Cercocebus torquatus*: an application of three-dimensional geometric morphometric techniques to the study of morphological variation. J Anat 193:251–272.

Peters CR. 1987. Nut-like oil seeds—food for monkeys, chimpanzees, humans, and probably ape-men. Am J Phys Anthropol 73: 333–363.

Picq PG. 1990. L'articulation Temporo-mandibulaire des Hominidés. Paris: Le Centre National de la Recherche Scientifique.

Piperno DR. 2006. Phytoliths: a comprehensive guide for archeologists and paleoecologists. Lanham MD: AltaMira Press.

Popowics TE, Herring SW. 2007. Load transmission in the nasocrontal suture of the pig, *Sus scrofa*. J Biomech 40:837–844.

Prendergast HDV, Hattersley PW, Stone NE, Lazarides M. 1986. C_4 acid decarboxylation type in *Eragrostis* (Poaceae) patterns of variation in chloroplast position, ultrastructure and geographical distribution. Plant Cell Environ 9:333–344.

Rabenold D, Pearson OM. 2011. Abrasive, silica phytoliths and the evolution of thick molar enamel in primates, with implications for the diet of *Paranthropus boisei*. PLoS One 6:e28379.

J_ID: AR Customer A_ID: AR23073 Cadmus Art: AR23073 Ed. Ref. No.: 14-0304 Date: 30-October-14 Stage: Page: 22

Rak Y. 1983. The australopithecine face. New York: Academic Press.

Ross CF, Berthaume MA, Dechow PC, Iriarte-Diaz J, Porro LB, Richmond BG, Spencer M, Strait D. 2011. *In vivo* bone strain and finite-element modeling of the craniofacial haft in catarrhine primates. J Anat 218:112–141.

Sage RF, Christin P-A, Edwards EJ. 2011. The C4 plant lineages of planet Earth. J Exp Bot 62:3155–3169.

Schwartz-Dabney CL, Dechow PC. 2002. Accuracy of elastic property measurement in mandibular cortical bone is improved by using cylindrical specimens. J Biomech Eng 124:714–723.

Schwartz-Dabney CL, Dechow PC. 2003. Variations in cortical material properties throughout the human dentate mandible. Am J Phys Anthropol 120:252–277.

Scott RS, Teaford MF, Ungar PS. 2012. Dental microwear texture and anthropoid diets. Am J Phys Anthropol 147:551–579.

Scott RS, Ungar PS, Bergstrom TS, Brown CA, Grine FE, Teaford MF, Walker A. 2005. Dental microwear texture analysis shows within-species diet variability in fossil hominins. Nature 436:693–695.

Singleton M. 2002. Pattern of cranial shape variation in the Papionini (Primates: Cercopithecinae). J Hum Evol 42:547–578.

Smith RJ. 1978. Mandibular biomechanics and temporomandibular joint function in primates. Am J Phys Anthropol 49:341–350.

Smith AL, Benazzi S, Ledogar JA, Tamvada K, Smith LC, Weber GW, Spencer MA, Dechow PC, Grosse IR, Ross CF, Richmond BG, Wright BW, Wang Q, Byron C, Slice DE, Strait DS. Biomechanical implications of intraspecific shape variation in chimpanzee crania: moving towards an integration of geometric morphometrics and finite element analysis. Anat Rec, in press.

Spencer MA. 1995. Masticatory system configuration and diet in anthropoid primates [Dissertation]. Stony Brook (NY): State University of New York at Stony Brook.

Spencer MA. 1998. Force production in the primate masticatory system: electromyographic tests of biomechanical hypotheses. J Hum Evol 34:25–54.

Spencer MA. 1999. Constraints on masticatory system evolution in anthropoid primates. Am J Phys Anthropol 108:483–506.

Strait DS, Constantino P, Lucas PW, Richmond BG, Spencer MA, Dechow PC, Ross CF, Grosse IR, Wright BW, Wood BA, et al. 2013. Diet and dietary adaptations in early hominins: the hard food perspective. Am J Phys Anthropol 151:339–355.

Strait DS, Grine FE. 2004. Inferring hominoid and early hominid phylogeny using craniodental characters: the role of fossil taxa. J Hum Evol 47:399–452.

Strait DS, Richmond BG, Spencer MA, Ross CF, Wood BA. 2007. Masticatory biomechanics and its relevance to early hominid phylogeny: an examination of palate thickness using finite element analysis. J Hum Evol 52:589–599.

Strait DS, Wang Q, Dechow PC, Ross CF, Richmond BG, Spencer MA, Patel BA. 2005. Modeling elastic properties in finite element analysis: how much precision is needed to produce an accurate model? Anat Rec A 283:275–287.

Strait DS, Weber GW, Neubauer S, Chalk J, Richmond BG, Lucas PW, Spencer MA, Schrein C, Dechow PC, Ross CF, et al. 2009. The feeding biomechanics and dietary ecology of *Australopithecus africanus*. Proc Natl Acad Sci USA 106:2124–2129.

Strait DS, Wright BW, Richmond BG, Ross CF, Dechow PC, Spencer MA, Wang Q. 2008. Craniofacial strain patterns during premolar loading: implications for human evolution. In: Vinyard CJ, Ravosa MJ, Wall CE, editors. Primate craniofacial function and biology. New York: Springer. p 173–198.

Strömburg CAE, Dunn RE, Madden RH, Kohn MJ, Carlini AA. 2013. Decoupling the spread of grasslands from the evolution of grazer-type herbivores in South America. Nat Comm 4:1478.

Taylor AB, Vinyard CJ. 2013. The relationship among jaw-muscle fiber architecture, jaw morphology and feeding behavior in extant apes and modern humans. Am J Phys Anthropol 151:120–134.

Teaford MF, Ungar PF. 2000. Diet and the evolution of the earliest human ancestors. Proc Natl Acad Sci USA 97:13506–13511.

Tobias PV. 1967. The cranium and maxillary dentition of *Australopithecus* (Zinjanthropus) boisei. Olduvai Gorge, Vol. 2. Cambridge: Cambridge Univ Press.

Ungar PS, Grine FE, Teaford MF. 2008. Dental microwear and diet of the Plio-Pleistocene hominin *Paranthropus boisei*. PLoS One 3: e2044.

Ungar PS, Sponheimer M. 2011. The diets of early hominins. Science 334:190–193.

Van der Merwe NJ, Masao FT, Bamford MK. 2008. Isotopic evidence for contrasting diets of early hominins *Homo habilis* and *Australopithecus boisei* of Tanzania. S Afr J Sci 104:153–155.

Walker A. 1981. Diet and teeth—dietary hypotheses and human-evolution. Phil Trans R Soc Lond B 292:57–64.

Walker A, Leakey REF, Harris J, Brown F. 1986. 2.5-Myr *Australopithecus boisei* from west of Lake Turkana, Kenya. Nature 322: 517–522.

Wang Q, Wood SA, Grosse IR, Ross CF, Zapata U, Byron CD, Wright BW, Strait DS. 2012. The role of the sutures in biomechanical dynamic simulation of a macaque cranial finite element model: implications for the evolution of craniofacial form. Anat Rec 295:278–288..

Weber GW, Bookstein FL, Strait DS. 2011. Virtual Anthropology meets biomechanics. J Biomech 44:1429–1432.

Wood SA, Strait DS, Dumont ER, Ross CF, Grosse IR. 2011. The effects of modeling simplifications on craniofacial finite element model: the alveoli (tooth sockets) and periodontal ligaments. J Biomech 44:1831–1838.

Wroe S, Ferrara TL, McHenry CR, Curnoe D, Chamoli U. 2010. The craniomandibular mechanics of being human. Proc R Soc Lond B 277:3579–3586.

Yeakel JD, Dominy NJ, Koch PL, Mangel M. 2013. Functional morphology, stable isotopes, and human evolution: a model of consilience. Evolution 68:190–203.

Zienkiewicz OC, Taylor RL, Zhu JZ. 2005. The finite element method: its basis and fundamentals. 6th ed. Amsterdam: Butterworth-Heinemann.

APPENDIX : MATERIAL PROPERTIES OF GRASS AND SEDGE SEEDS

Frank Mbago of the Herbarium of the University of Dar es Salaam gathered grass and sedge seeds growing wild in Tanzania. No permits were required for the described study, which complied with all relevant regulations, and none of the species sampled are protected. The data for grass caryopses ("grains") refer to the pericarp adherent to the true thin seed coat. The data for sedge fruits refers to homologous layers, although these are non-adherent. Mechanical tests on both were made by setting them in resin and exposing their outermost tissues by very light polishing on the resin surface. SEM imaging showed that the pericarp, and often the seed coat, is composed of fibers, forming a very thin husk (Supporting Information Fig. A1). We targeted both tissues with a Berkovich tip on a Hysitron Ubi1 nanoindenter using forces of 300–450 μN with the aim of obtaining values for indentation hardness and the reduced elastic modulus. We assumed an Oliver–Pharr analysis (Lucas et al., 2012). Mechanical measurements (Table 5) were variable for a variety of reasons. One was the difficulty of ascertaining exactly how thick the supporting tissue was under the indenter. Also, the optics on current nanoindenters is not adequate to identify layers accurately prior to testing. Thus, there is always the possibility of missing the target. To minimize error, the specimen surfaces were scanned pre-test with the Berkovich tip at 2 μN force. In addition, post-test force–displacement curves that suggested that the

ID: chandrasekar.v Time: 20:57 I Path: N:/3b2/AR##/Vol00000/140193/APPFile/JW-AR##140193

J_ID: AR Customer A_ID: AR23073 Cadmus Art: AR23073 Ed. Ref. No.: 14-0304 Date: 30-October-14 Stage: Page: 23

indenter glanced against the edges of the target, or were indented on a strongly inclined surface or which the curve showed were heterogeneous, were deleted. The dataset was also examined for outliers. Some of the remaining variability is probably due to varying orientations of the fibers to the indenter (as in *Mezzettia parviflora* seed shell) (Lucas et al., 2012). As a counterweight to this in Table 5, the total range for moduli and hardness values is given along with means and standard deviations.

Seed dimensions are for whole fruits (Supporting Information Fig. A1), except for *Carex monostachya* where the measurements were made on bare seeds. Length and width were measured with an optical stereo microscope; thickness with a digital screw-gage micrometer (reading to 0.001 mm). Moisture content was determined by oven-drying a large number of whole seeds at 60°C until constant weight. Moisture content (%dry wt) was calculated as [(mass of water/total mass of dry solids) × 100]. Moisture contents are "as tested in the nanoindenter," and will be lower than those in the field. The moisture contents given here will also likely underestimate values that could be obtained by comminuting seeds prior to drying. However, since most of the moisture would be in the endosperm and embryo inside the protective "shell," we think that the current dataset is accurate with respect to mechanically protective tissues. Material and mechanical properties of seeds are given in Table 5. Note that for all of these species, the hardness (H) values are similar to or only slightly less than those of the much larger *M. parviflora* (Annonaceae), the most obdurate seed known in the literature (Lucas et al., 2012). Yet, none of these seeds approach the hardness of grass phytoliths (*Ampelodesmos mauritanicus,* $H = 2{,}560$ MPa), tooth enamel ($H = 5{,}000$ MPa), or quartz dust ($H = 12{,}800$ MPa) (Lucas et al., 2013). Phytoliths are not hard enough to abrade enamel (Lucas et al., 2013), so it follows that the same is true of seed shells, although it remains to be seen if some shells might be hard enough to mark enamel non-abrasively.

SEM studies of these seeds included energy dispersive spectroscopy (EDS) for elemental analysis (Supporting Information Fig. A2). This showed that the husks of all of these seeds contain phytoliths. The quantities in *Cyperus bulbosus* and *Pennisetum stramineum* were so great as to effectively render them armored. It is reasonable to expect, therefore, that the consumption of grass and sedge seeds will deliver phytoliths into the oral cavity. All of the species studied (Table 5) utilize the C4 photosynthetic pathway except for *Carex monostachya* (e.g., Hesla et al., 1982; Prendergast et al., 1986; Christin et al., 2009; Sage et al., 2011). AQ2

AQ1: Please note that the following reference citations are not detailed in the reference list: Greaves, 1998; Lucas, 2004; Strait et al., 2010; Dumont et al., 2005; Keyak and Rossi; Lucas et al., 2009. Kindly provide or delete the citations.

AQ2: Please spell out "SEM."

AQ3: The following references are not cited in the text: McNulty et al., 2006; Mitteroecker et al., 2004; O'Higgins and Jones, 1998; Singleton, 2002. Please cite or delete the references from the list.

AQ4: Please update reference "Smith et al." in list as well as in text.

AQ5: Please specify whether reference "Spencer, 1995" is master's or doctoral dissertation.

AQ6: Please provide complete list of author names for reference "Strait et al., 2013, 2009."

AQ7: Please check whether the year of publication added is OK as set.

AQ8: Please note that Appendix Figures A1 and A2 have been treated as Supporting Information. Kindly confirm.

AQ9: Please check whether the grant information is OK as set.